Arabian Journal for Science and Engineering (2023) 48:16167–16185
https://doi.org/10.1007/s13369-023-08073-4

RESEARCH ARTICLE-CHEMICAL ENGINEERING

Construction, Characterization, DFT Computational Study, and Evaluation the Performance of Some New *N*-Amino Pyridinone Schiff Base Catalyzed with Ceric(IV) Ammonium Nitrate (CAN) as Corrosion Inhibitors in Some Petroleum Applications

Gehad A. Abd-elmaksoud[1] · Moustafa S. Abusaif[2] · Yousry A. Ammar[2] · S. Al-Sharbasy[1] · M. A. Migahed[3]

Received: 1 February 2023 / Accepted: 15 June 2023 / Published online: 12 July 2023

Abstract
In this paper, two novel organic inhibitors, TAP-TPP and TAP-CEQ, were prepared via Schiff base condensation as a green chemistry methodology using an eco-friendly catalyst, ceric ammonium nitrate, with a high yield (87% and 91%), and characterized via elemental analysis, FTIR, ^{1}H, and ^{13}C NMR spectroscopic analysis tools. Weight loss assessment was utilized as a chemical testing method, and the maximum inhibition efficiency of TAP-TPP and TAP-CEQ is 89.4% and 91.8%, respectively. PDP and EIS were electrochemical measures to determine the efficacy of both inhibitors as anticorrosion for carbon steel alloys in 2 M HCl aggressive media. The collected electrochemical results demonstrated that both inhibitors behaved as excellent anticorrosion agents for metallic constructions. According to the potentiodynamic polarization (PDP) analysis, these organic inhibitors worked as mixed-type inhibitors. The adsorption isotherm revealed that undertaken compounds obeyed Langmuir adsorption isotherm with the free energies of adsorption of ranged from $\Delta G = -34.29$ to -34.63 kJ Mol^{-1}. Also, electrochemical impedance spectroscopy (EIS) data confirmed that the values charge transfer resistance (R_{ct}) was increased by increasing the concentration of the injected inhibitor molecules. In contrast, the electrochemical double layer (C_{dl}) was dramatically decreased. The work was supported by two-surface analysis methods such as SEM and EDX. For more details, the values of percentage inhibition efficiency can be ordered as follows: TAP-CEQ > TAP-TPP. Finally, a suitable inhibition mechanism and theoretical studies including E_{HOMO}, E_{LUMO}, diploe moment (μ), and electrophilicity index (ω) were assumed and discussed in detailed.

Keywords *N*-amino pyridinone derivatives · Carbon steel · Potentiodynamic polarization · EIS · EDX · SEM · Adsorption

List of symbols

TAP-CEQ	6-Amino-1-(((2-chloro-7-ethoxyquinolin-3-yl)methylene)amino)-2-oxo-4-(thiophen-2-yl)-1,2-dihydropyridine-3,5-dicarbonitrile
TAP-TPP	6-Amino-2-oxo-1-(((1-phenyl-3-(p-tolyl)-1*H*-pyrazol-4-yl)methylene)amino)-4-(thiophen-2-yl)-1,2-dihydropyridine-3,5-dicarbonitrile
CAN	Ceric ammonium nitrate
^{1}H NMR	Proton nuclear magnetic resonance
PDP	Potentiodynamic polarization
R_{ct}	Charge transfer resistance
SEM	Scanning electron microscope
E_{LUMO}	Higher occupied molecular orbital energy
ω	Electrophilicity index
FTIR	Fourier transform infrared spectroscopy
^{13}C NMR	Carbon nuclear magnetic resonance
EIS	Electrochemical impedance spectroscopy
C_{dl}	Electrochemical double layer
E_{HOMO}	Higher occupied molecular orbital energy
μ	Diploe moment

✉ Moustafa S. Abusaif
mostafahozaifa317@azhar.edu.eg

[1] Department of Chemistry, Faculty of Science (Girls), Al-Azhar University, Nasr City, Cairo 11884, Egypt

[2] Department of Chemistry, Faculty of Science (Boys), Al-Azhar University, Nasr City, Cairo 11884, Egypt

[3] Egyptian Petroleum Research Institute (EPRI), Nasr City, Cairo 11727, Egypt

1 Introduction

Metals corrosion can be regarded as one of the most serious problems in the petroleum sector, including the chemical cleaning of heat exchangers to dissolve inorganic scales and the acidization of old oil and gas wells. Such an acidization process includes pumping acid solution into the wellbore to increase the produced oil or gas flow rate [1]. Generally, the hydrochloric acid solution is used in this method [2]. The problem now is the corrosive nature of this kind of inorganic acids, which depends on various factors such as pH, temperature, and dissolved gases [3–5]. From the economic point of view, one of the most effective tools for mitigating metal corrosion is injecting the corrosive fluid with a sufficient dose of a suitable type of effective corrosion inhibitor [4–7]. Numerous reviews about different types of organic inhibitors have already been reported [8–12]. It was reported that the organic additives containing heteroatoms such as N, O, S, and P displayed significant inhibition efficiency toward the corrosion process due to their ability to supply lone pair electrons to such metal surfaces. Other factors include the type of aromatic ring and unsaturated bonds [13, 14]. The greatest manufactured organic molecules, practically those containing pyridone derivatives, are less expensive, environmentally sustainable, and suitable for use as corrosion inhibitors in acidic environments [15–17]. Also, it is a useful method to use an eco-friendly catalyst in the synthetic pathways of organic pyridinone Schiff base derivatives (green chemistry), such as ceric ammonium nitrate that can be applied as Lewis's acid or oxidizing substance [18–22]. The corrosion inhibition mechanism of such organic additives works by adsorption of these organic additives on the surface of metals. Also, it depends on the nature of the zero-charge potential of the steel surface [23]. Carbon steel alloys are regarded as the most widely used materials in all industrial processes. This can be attributed to their excellent mechanical properties and low production cost [24]. Generally, acidic solutions have many uses in various industrial applications such as acidizing of old oil wells, removal of inorganic hard scales in heat exchangers, and pickling of metal surface [25]. Hydrochloric acid is regarded as one of the most important inorganic acids used in such processes, which can cause serious metallic corrosion [26]. Normally, chemical inhibition using specific types of organic compounds acts through a film-forming mechanism [27]. In addition, pyridinone derivatives are the most active component used as anti-inflammatory and antimicrobial drugs and possess unique biological capabilities while posing no considerable environmental dangers [28–30]. In the present work, the target is aimed to design and synthesize two novel *N*-amino pyridinone derivatives linked to pyrazole or quinoline moieties via Schiff's base, TAP-TPP, and TAP-CEQ (as shown in Scheme 1) and confirm their chemical structures using various spectroscopic techniques. Furthermore, the investigation of the pyridinone derivatives an anticorrosive agent for CS in a hydrochloric acid medium was assessed using chemical and electrochemical (EIS and PDP) methods. Also, SEM and EDX studies were used to examine the CS morphology without and with inhibitor molecules.

2 Experimental Section

2.1 Synthesis of the Target Organic Compounds

The melting values of the novel prepared pyridinone derivatives TAP-TPP and TAP-CEQ were determined and reported on the digital Gallen Kamp MFB-595 instrument. Also, their FTIR spectra were analyzed using the Shimadzu 440 spectrophotometer at the range 400–4000 cm^{-1}. A Bruker (400 and 101 MHz) spectrometer is used to evaluate the ^{1}H and ^{13}C signals in the NMR spectra and is recorded relative to deuterated solvent signals only in dimethyl sulfoxide (DMSO-*d*6).

2.1.1 Synthesis of 1,6-Diamino-2-oxo-4-(Thiophen-2-yl)-1,2-Dihydropyridine-3,5-Dicarbonitrile (TAP)

The starting material TAP was prepared as stated in the literature method [31]. To a solution of cyan acetic hydrazide (5 mmol) and 2-(thiophen-2-ylmethylene) malononitrile (5 mmol) in ethanolic solution (20 mL) catalyzed with a mixture of CH_3COONH_4 (2 mmol)/CAN (1 mmol), the solution was refluxed for 1 h until the precipitated formed on hot. The obtained solid product was collected by filtration, then dried, and recrystallized by dioxane. The relevant synthetic reaction is shown in Scheme 1.

2.1.2 Synthesis of Organic Schiff's Bases Derivatives (TAP-TPP and TAP-CEQ)

Method (i): Using Acetic Acid as a Catalyst To a solution of the starting material TAP (1 mmol, 0.25 g) and the formyl derivatives (1 mmol) (namely, 1-phenyl-3-(p-tolyl)-1H-pyrazole-4-carbaldehyde and 2-chloro-7-ethoxyquinoline-3-carbaldehyde) in (20 mL) dioxane solution catalyzed with glacial AcOH (1 mL) and then refluxed for 3 h (TLC monitoring), the mixture was allowed to cool and treated with ethyl alcohol, and then the precipitate was filtered, washed by ethyl alcohol, dried, and recrystallized from CH_3CN to give the required pure pyridinone derivatives TAP-TPP and TAP-CEQ. The structure of the product is shown in Scheme 1.

Method (ii): Using Ceric Ammonium Nitrate as a Catalyst A solution of organic compound TAP (1 mmol,

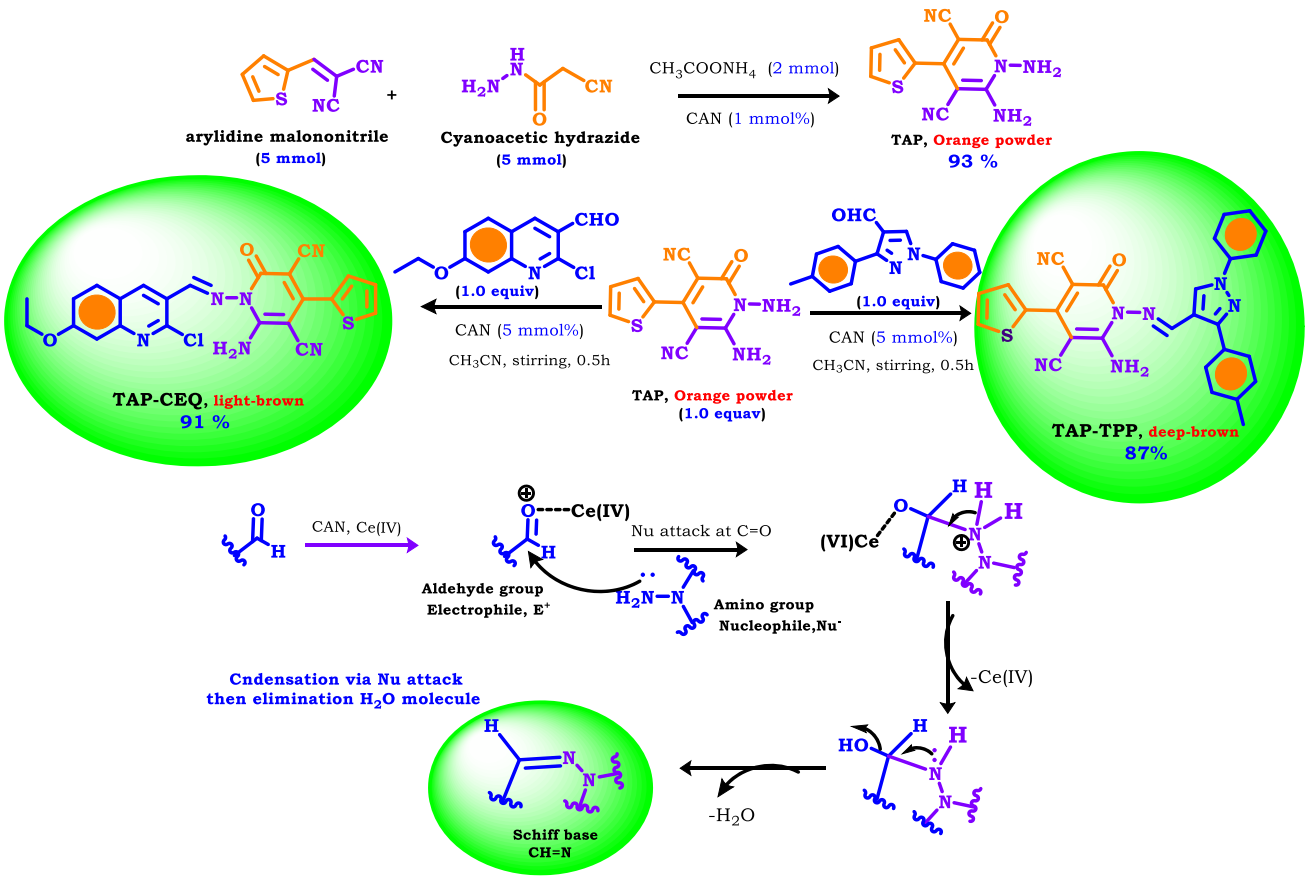

Scheme 1 Synthetic pathway for the preparation of two novel inhibitors TAP-TPP, TAP-CEQ and their Schiff's base mechanism using cerium ammonium nitrate (CAN)

0.25 g) and the appropriate 1-phenyl-3-(p-tolyl)-1H-pyrazole-4-carbaldehyde and 2-chloro-7-ethoxyquinoline-3-carbaldehyde (1 mmol) in (10 mL) acetonitrile solution catalyzed by adding cerium ammonium nitrate (5 mmol%), the solution was stirred at room for 0.5 h until the solution becomes clear time and then formed a color solid precipitated. The solid was washed with ethyl alcohol and recrystallized from CH_3CN to give the required pure pyridinone derivatives TAP-TPP and TAP-CEQ.

2.1.3 6-Amino-2-Oxo-1-(((1-Phenyl-3-(p-tolyl)-1*H*-Pyrazol-4-yl)methylene)amino)-4-(Thiophen-2-yl)-1,2-Dihydropyridine-3,5-Dicarbonitrile (TAP-TPP)

Pale gray powder; yield = 82%; M.p. = 340–342 °C; IR (KBr): ν_{max} = 3421, 3315 (NH_2), 3040 (CH-arom.), 2920 (CH-aliph.), 2211 (2CN), 1654 (C=O), 1610 (CH=N) (Fig. 1); ^{1}H NMR (δ, ppm) 2.39 (3H, s, $\underline{CH_3}$.tolyl), 7.28 (1H, t, J = 8.8 Hz, CH_{arom}), 7.36 (d, J = 8.0 Hz, CH_{arom}), 7.46 (t, J = 7.4 Hz, 1H, CH_{arom}), 7.61 (t, J = 7.9 Hz, 2H, CH_{arom}), 7.57 (2H, d, J = 6.4 Hz, 1H, CH_{arom}), 7.65 (2H, d, J = 8.0 Hz, CH_{arom}), 7.95 (1H, d, J = 6.4 Hz, CH_{arom}), 8.00 (2H, d, J = 7.7 Hz, CH_{arom}), 8.44 (2H, s, br.NH_2; D_2O exchangeable), 8.97 (1H, s, CH_{arom}), 9.44 (1H, s, methylinic-$\underline{CH}$); (Fig. 2) ^{13}C NMR (δ, ppm) 21.36 (CH_3), 90.70 ($\underline{C}$–CN), 115.09, 115.36 (2CN), 116.53, 116.68, 117.07, 117.12, 117.26, 119.07, 119.28, 119.66, 127.37, 128.36, 128.73, 128.94, 129.07, 129.13, 130.02, 130.30, 130.91, 131.09, 133.61, 133.82, 135.39, 138.34, 139.19, 139.55, 151.15, 151.98, 152.52, 154.54 (Ar.Cs), 154.69 (CH=N), 157.22 ($\underline{C}$-NH_2), 165.38 (C=O) (Fig. 2).

2.1.4 6-Amino-1-(((2-Chloro-7-Ethoxyquinnolin-3-yl) Methylene) Amino)-2-Oxo-4-(Thiophen-2-yl)-1,2-Dihydropyridine-3,5-Dicarbonitrile (TAP-CEQ)

yellow powder; yield = 84%; M.p. = 351–353 °C; IR (KBr): ν_{max} = 3464, 3283 (NH_2), 2984 (CH-aliph.), 2215 (2CN), 1677 (C=O), 1614 (CH=N); (Figure S1) ^{1}H NMR (δ, ppm) 1.44 (3H, t, $\underline{CH_3}CH_2O$), 4.27 (2H, q, $CH_3\underline{CH_2}O$), 7.29 (1H, t, J = 8.4 Hz, CH-thiophene), 7.39 (1H, s, CH_{arom}), 7.42 (1H, d, J = 9.5 Hz, CH_{arom}), 7.56 (1H, d, J = 9.4 Hz, CH_{arom}), 7.69 (2H, d, J = 8.9 Hz, CH-thiophene), 8.16 (1H, s, -CH-Q_4), 8.58 (2H, s, br.NH_2; D_2O

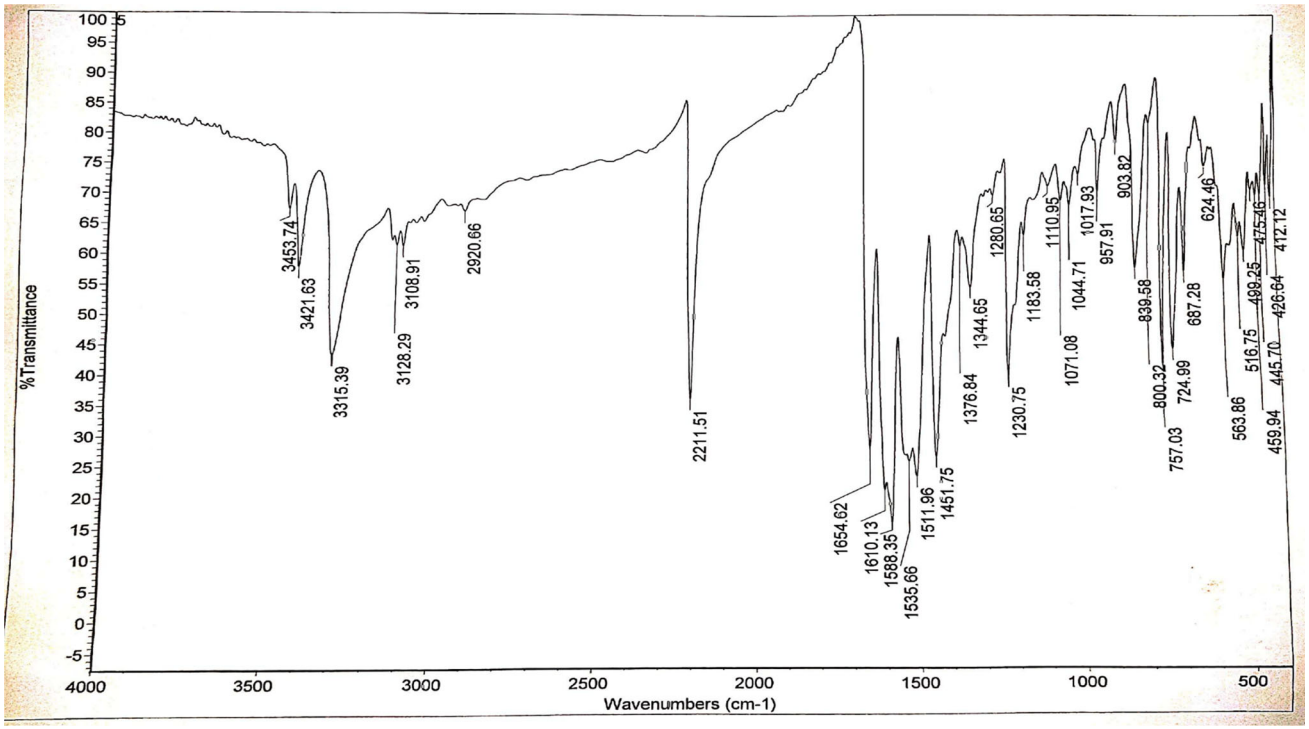

Fig. 1 FTIR spectrum of compound (TAP-TPP)

exchangeable), 9.36 (IH, s, methylinic-CH); (Figure S2) ^{13}C NMR (δ, ppm) 14.89 (CH_3CH_2O), 64.34 (CH_3CH_2O), 90.93 (C–CN), 107.30, 107.64, 115.40, 116.12 (2CN), 116.51, 121.09, 122.15, 127.04, 128.33, 130.23, 131.02, 131.19, 131.52, 133.46, 138.67, 148.88, 149.59, 152.70, 153.61 (Ar-Cs), 154.66 (CH = N), 161.70 (C-NH_2), 163.19 (C-OEt), 168.58 (C=O) (Figure S3).

2.2 Corrosion Measurements

2.2.1 Weight Loss Measurements

Corrosion experiments were conducted on CS alloy (density = 7.86 g cm^{-3}) with the following chemical composition (wt. %): C, 0.025; S, 0.03; Si, 0.15; N, 0.27; Mn, 1.52; Ni, 0.16; Cr, 0.26; Al, 0.38; Cu, 0.24; Ti, 0.13; Nb, 0.92; and the rest is Fe. The aggressive medium of 2 M HCl solution was newly prepared by dilution of analytical grade concentrated hydrochloric acid using bi-distilled water. The dose of the two inhibitors (TAP-TPP and TAP-CEQ) in the aggressive medium ranged from 30 to 150 ppm, respectively. The carbon steel alloy with dimension 3 cm × 2 cm × 0.2 cm was abraded with several sandpapers with different grades ranging from 360 to 3000. The grasses present on the surface were removed by acetone, washed with deionized water and dried with an air drier, and immersed in an aggressive medium. After weighing exactly, samples were submerged in a glass container containing 200 ml of the corrosive medium with and without various doses of the pyridinone inhibitors. After immersion time (24 h), the test specimens were detached from the beaker, washed with bi-distilled water, dried, and finally weighed. The percentage inhibition effectiveness obtained from the weight loss technique (IE_w %) and the rate of corrosion (CR) in (mg cm^{-2} h^{-1}) had been estimated via Eqs. 1 and 2 [32, 33]:

$$IE_w(\%) = \theta \times 100 = \left(\frac{CR - CR_i}{CR}\right) \times 100 \quad (1)$$

$$CR = \frac{\Delta W}{St} \quad (2)$$

where CR and CR_i are the values of the rate of corrosion in an aggressive medium without and with various doses of the used inhibitors, respectively. The value of average weight loss expressed in (mg) for three parallel CS specimens is represented in ΔW, S is the average area of the sample expressed cm^2, and t is referred to the duration time expressed h.

2.2.2 Electrochemical Studies

All EIS and PDP experiments were accomplished via Volta lab 80 potentiostat (model PGZ − 402). A conventional electrochemical with three electrodes was used in all electrochemical tests. Carbon steel alloy was used as a working specimen, Pt wire was used as a counter electrode, and SCE was used as a reference electrode [34, 35]. For EIS tests, an

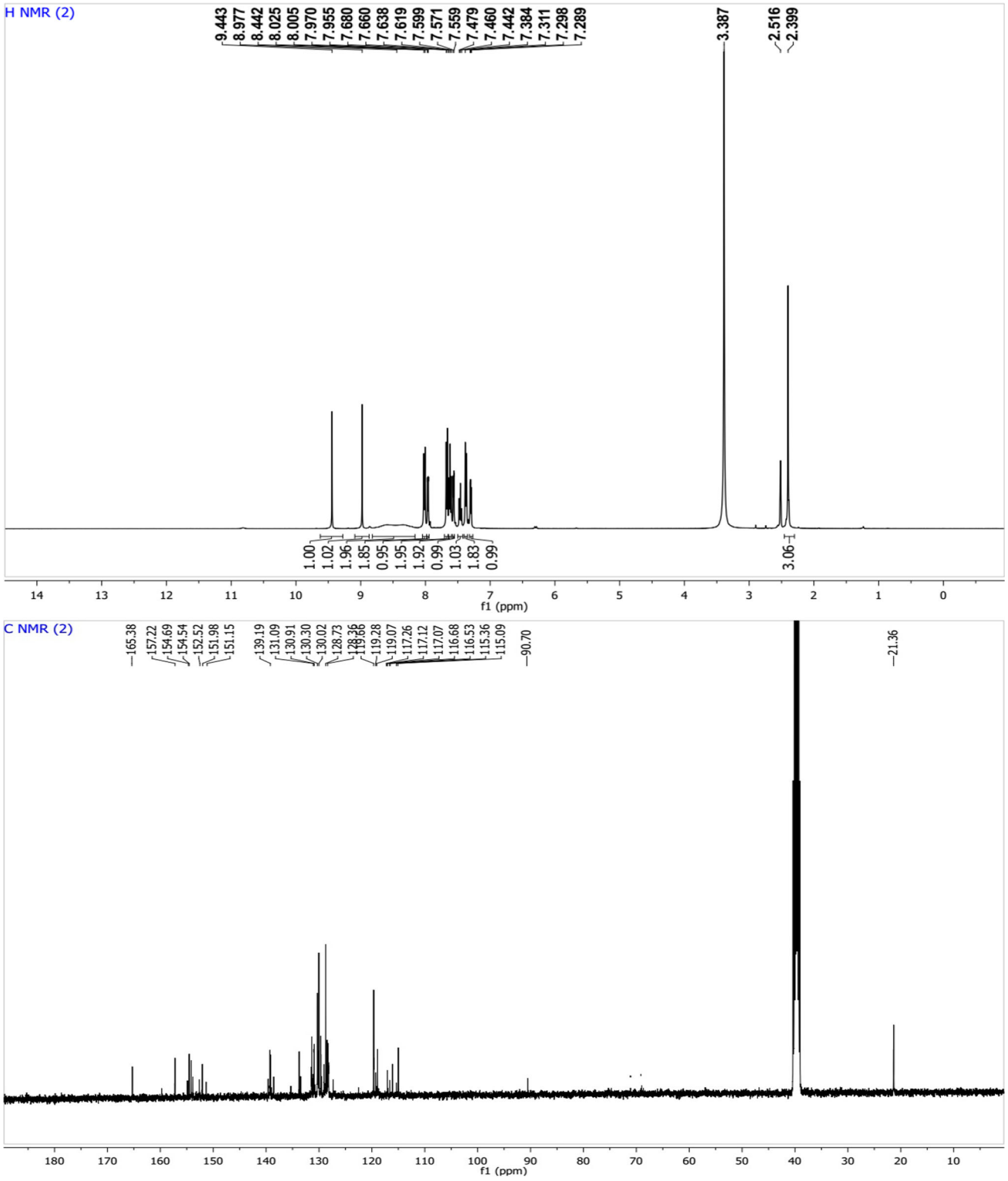

Fig. 2 ^{1}H NMR and ^{13}C NMR spectrum of compound (TAP-TPP)

AC signal with 10 mV peak to peak was applied in a potentiostat mode at OCP, in the range of frequencies between 10^5 Hz and 0.5 Hz [24]. PDP experiments were performed at a scan rate of 1 mV s^{-1} and sweeping the applied potential in the average of ± 250 mV with respect to OCP [36–38]. For consistency and accuracy, all tests were carried out three times and the average results were recorded.

2.3 Surface Analysis

Surface morphology of carbon steel alloys, with dimensions 12 × 12 × 2 mm, without and after immersion of 150 ppm of the synthesized pyridinone derivatives for 24 h in 2 M HCl, was investigated by SEM. The nature of the adherent protective layer on CS alloy was tested by a Zeiss E_{vo} 10 device attached to the EDX system [38]. The power beam accelerating voltage was 25 kV. The micrographs of the carbon steel alloys were taken at a magnification power of (×1500).

2.4 Computational Study (DFT Calculation)

The DFT calculation for organic dye TAP-TPP and TAP-CEQ was performed by using Gaussian 09 and Gaussian view 6.0 software [39, 40]. The calculations, including frontier molecular orbital and MEPs, were carried out using popular hybrid functional B3LYP functional with the double zeta basis set 6–31 g (d) for optimization of the molecule according to the previously reported methods [41, 42].

3 Result and Discussion

3.1 Chemistry (Synthesis, Structure Elucidation, and Physical Properties of Inhibitors)

3.1.1 Synthesis and Structure Elucidation of Inhibitors

In this manuscript, we have employed a clean and rapid ceric ammonium nitrate CAN-catalyzed synthesis of novel organic Schiff base inhibitors TAP-TPP and TAP-CEQ which are displayed in Schemes 1. Firstly, the *N*-amino pyridinone derivatives TAP is employed as the starting material formed according to the literature method [31] via cyclocondensation by reaction of 2-(thiophen-2-ylmethylene) malononitrile with cyanoacetohydrazide in ethyl alcohol solution catalyzed with a mixture of ammonium acetate and cerium ammonium nitrate CAN (Scheme 1). Furthermore, the nucleophilic substitution reaction between the starting material TAP and two specified heterocyclic aldehydes was investigated using two different methods. The first method was known as the classical and hazard method, and it is employed by the refluxing of the *N*-amino pyridinone derivatives TAP and the appropriate aldehydes in a dioxane solution catalyzed with glacial acetic acid for about 3 h. The yield of the Schiff base produced ranged from 65 to 68% while the second method was employed by the stirring of the *N*-amino pyridinone derivatives TAP and the appropriate aldehydes in acetonitrile solution catalyzed with ceric ammonium nitrate CAN (5 mmol %) for only 0.5 h at room temperature, and the yield of two organic inhibitors TAP-TPP and TAP-CEQ was increased into 87% and 91%, respectively (Scheme 1). Generally, the advantage of this reaction in the case of using CAN as a catalyst is that the reaction occurred at room temperature for a short time and without hazardous catalyst (green chemistry) with excellent yield, compared with the classical method that completed through refluxing the reaction in the presence of acetic acid as catalyst (hazards catalyst) for a long time with a moderate yield.

Continuously, the spectroscopic data, IR, ^{1}H NMR, ^{13}C NMR, and elemental analysis are in accordance with the suggested structure. The IR spectra of the organic compound TAP-TPP exhibited sharp bands at ν 3421, 3315, 2211, 1654, 1610 cm^{-1} revealed to NH_2, CN, C=O, and new CH=N groups, respectively [43–46]. Their ^{1}H NMR spectra exhibited three singlet signals appearing at δ 2.39, 8.47, and 9.44 ppm significant to CH_3, NH_2, and methylinic-CH groups, respectively.^{13}C NMR spectra of the same compound presented new signals that appeared at δ 21.36, 15.09, 115.36, 154.69, and 165.38 ppm assigned to the CH_3, 2CN, methylinic-CH and C=O functions, respectively. Also, IR analysis of the compound (TAP-CEQ) showed significant stretching absorption bands at ν 3464, 3283 2215 cm^{-1}, which referred to NH_2 and cyano groups, respectively. Moreover, bands linked to carbonyl and CH-methylinic groups looked at ν 1677, and 1614 cm^{-1}, respectively. ^{1}H NMR spectra of compound (TAP-CEQ) exhibited two signals appeared at δ 1.44 ppm due to CH_3 protons, quartet signal at δ 4.27 ppm related to OCH_2 protons, and two singlet signals at δ 8.58 and 9.36 ppm associated to the amino group that canceled with D_2O and CH-methylinic group, respectively.

3.1.2 Physical Properties of Inhibitors

The physical properties of both organic inhibitors TAP-TPP and TAP-CEQ are listed in Table 1. Generally speaking, the color of organic dyes is slightly different (deep brown and light brown) compared with the intermediate TAP (orange crystal), which proves an elementary successful organic dyes formation. Next, both organic inhibitors TAP-TPP and TAP-CEQ recorded melting point 340–342 °C and 351–353 °C, respectively, higher than those of the intermediate TAP (285–287 °C).

Table 1 Physical properties and analytical data of organic inhibitors TAP-TPP and TAP-CEQ

Inhibitor	Mol. Wt.	Color	Yield (%)	MP (°C)	Found (Calculated)		
					%C	%H	%N
TAP-TPP	501.57 $C_{28}H_{19}N_7OS$	Deep brown	87	340–342	67.05 (67.02)	3.18 (3.82)	19.75 (19.55)
TAP-CEQ	474.92 $C_{23}H_{15}ClN_6O_2S$	Light brown	91	351–353	58.17 (58.02)	3.18 (3.29)	17.70 (17.97)

3.2 Weight Loss Studies

The weight loss method was a common practical method for determination of the percentage corrosion inhibition efficacy of the newly synthesized organic compounds. The dissolution behavior of CS in 2 M HCl solution in the absence and presence of different doses of pyridinone derivatives (TAP-TPP and TAP-CEQ) was considered via the weight loss technique, as shown in Fig. 3. The figure displays the rate of corrosion (CR) and inhibition effectiveness (IE_w %) of the synthesized pyridinone inhibitors. Figure 3 reveals that the values of corrosion rate are clearly reduced, and the values of percentage inhibition efficiency (IE_w %) are increased after adding various doses of pyridinone derivatives. Also, the maximum IE_w % values of TAP-TPP and TAP-CEQ are 89.4% and 91.8%, respectively. The behavior of the corrosion mitigation process by the pyridinone derivatives can be clarified on the basis of the adsorption of their particles on the CS surface, as stated by their stereochemistry.

3.3 Electrochemical Results

3.3.1 Potentiodynamic Polarization (PDP) Studies

Tafel polarization plots of carbon steel electrodes in aggressive solution without and with several doses of pyridinone derivatives (TAP-TPP and TAP-CEQ) were presented in Fig. 4. Electrochemical data were calculated by extrapolating Tafel curves and recorded in Table 2. As shown in Fig. 5, it is clear that by raising the dose of the used pyridinone derivatives, the recorded corrosion current density (i_{corr}) for the carbon steel alloy in the aggressive acidic solution displays a declining trend (i.e., strongly decrease). The addition of maximum concentration (i.e., 150 ppm) of the selected compounds produces a lowering of i_{corr} from 0.516 mA/cm^2 to 0.031 and 0.026 mA/cm^2 for both TAP-TPP and TAP-CEQ, respectively. This behavior proves the affinity of the synthesized pyridinone derivatives to reduce the corrosion rate and consequently increasing the percentage inhibition efficacy (IE %) [47]. By carefully investigating of Tafel curves, it is clear that both the anodic and cathodic Tafel lines were moved to more positive and negative directions about relation to the blank line. This behavior indicates that the adsorption of pyridinone compounds on CS surface decreases the cathodic hydrogen evolution and the iron anodic dissolution rate [48]. It had been seen that the values of cathodic and anodic Tafel slopes (β_a and β_c) remain almost unchanged without and with pyridinone derivatives and independent of the dose of inhibitor injected, indicating that the adsorption of the undertaken compounds on the CS alloy surface decreased value of corrosion rate without affecting on the corrosion mechanism. The distribution of the synthesized pyridinone derivatives on the CS alloy surface can be ascribed because of the interaction between the vacant d-orbital of the CS alloy surface and the lone pair electrons of O, N, and S atoms present in the pyridinone derivatives through electron type bonds. The corrosion inhibition occurs by forming a barrier layer that prevents metal dissolution. The percentage of inhibition effectiveness (IE_p) was estimated according to Eq. 3 [49–51].

$$IE_p = \left[\frac{i^0_{corr} - i_{corr}}{i^0_{corr}}\right] \times 100 \quad (3)$$

where i^0_{corr} and i_{corr} are the values of corrosion current density without and with the studied pyridinone derivatives.

The results in Table 2 confirmed that the change in the E_{corr} values was less than 85 mV/SCE, so that the nature of the absorption of the studied pyridinone derivatives (TAP-TPP and TAP-CEQ) was mixed-type inhibitors [52]. On the other hand, the inhibition action of pyridinone derivatives is enhanced by the existence of azo moiety, thiophene moiety, and lone pairs of electrons in the pyridinone inhibitors. Now, the values of percentage inhibition efficiency of the newly synthesized pyridinone derivatives can be ordered as follows: TAP-CEQ > TAP-TPP.

3.3.2 EIS Data and Their Explanations

For sure, the effectiveness of certain inhibitors can be established through AC impedance measurements. Accordingly, the EIS technique was applied in corrosion studies on various types of steel alloys [53]. In this work, the electrochemical behavior of CS alloy in an aggressive medium without and with several doses of the synthesized pyridinone derivatives

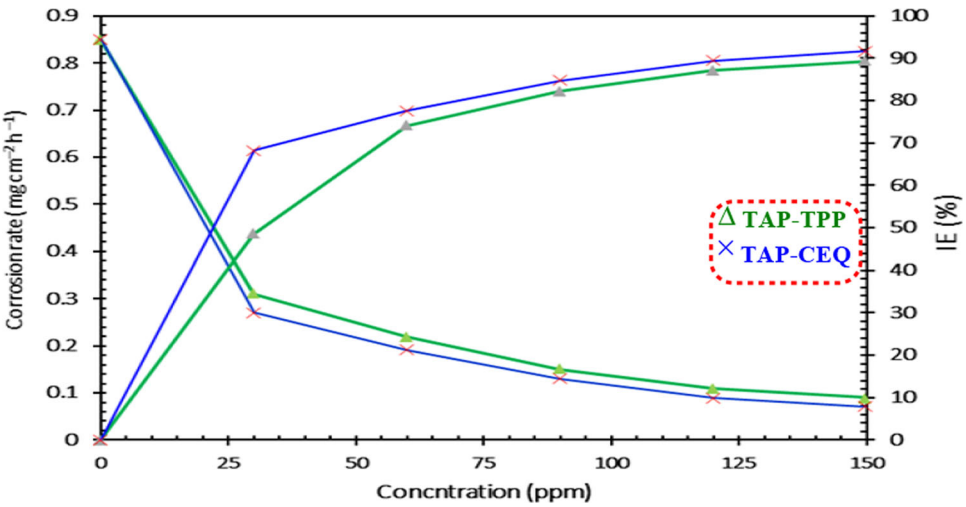

Fig. 3 Correlations between the corrosion rate and inhibition efficiency with various doses of compounds (TAP-TPP and TAP-CEQ)

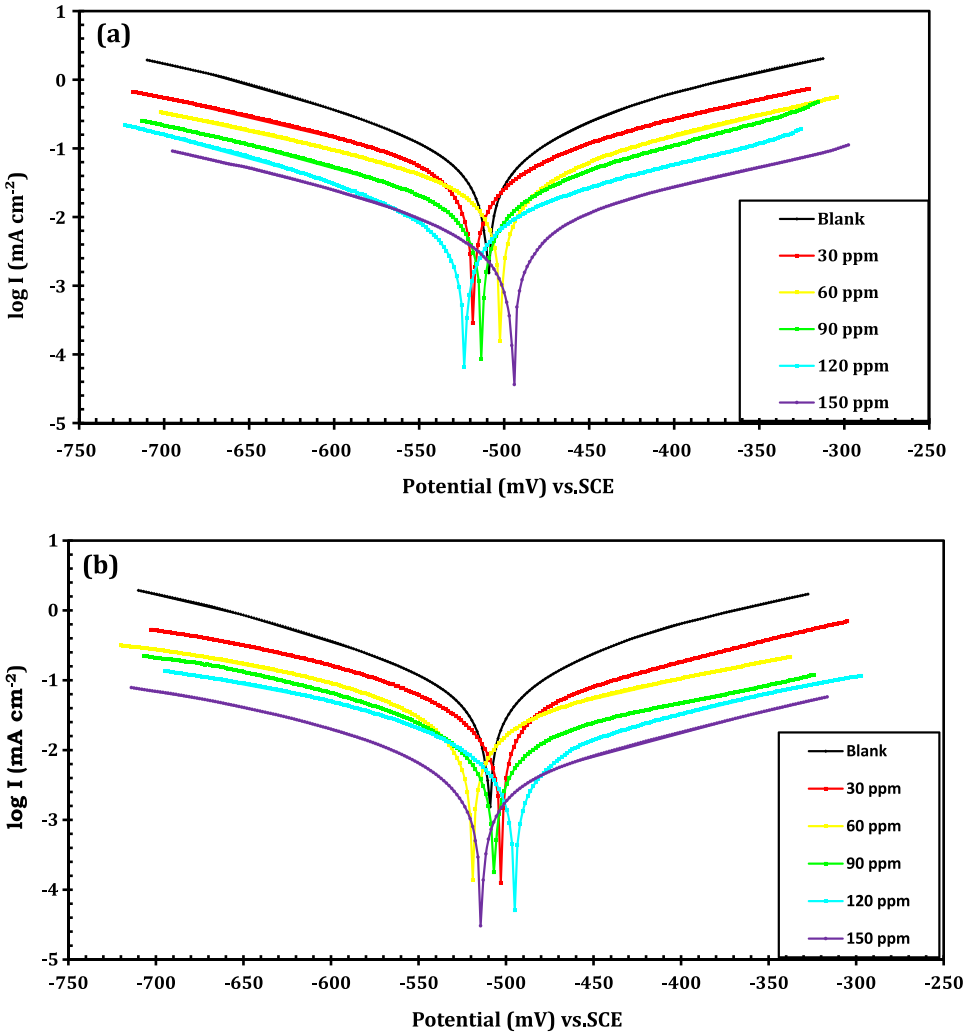

Fig. 4 Log I–E relationship for CS alloy in 2 M HCl without and with various doses of compounds: **a** TAP-TPP and **b** TAP-CEQ at 25 °C

Table 2 Electrochemical parameters obtained from the Tafel polarization tests on carbon steel alloy in 2 M HCl acidic solution without and with various inhibitors TAP-TPP and TAP-CEQ

Inhibitor	Conc. (ppm)	$-E_{corr.}$ mV (vs. SCE)	$I_{corr.}$ (mA cm^{-2})	β_a (mV dec^{-1})	$-\beta_c$ (mV dec^{-1})	θ	IE (%)
Blank	–	509.2	0.5163	107.2	149.5	–	–
TAP-TPP	30	497.1	0.2613	75.89	143.7	0.4939	49.39
	60	518.4	0.2037	106.1	164.3	0.6055	60.55
	90	502.5	0.1134	142.7	− 187.2	0.7804	78.04
	120	513.7	0.0682	98.3	154.7	0.8679	86.79
	150	523.2	0.0316	83.5	161.3	0.9388	93.88
TAP-CEQ	30	528.6	0.2481	171.3	− 146.2	0.5195	51.95
	60	503.1	0.1943	109.5	− 181.6	0.6237	62.37
	90	519.2	0.1026	125.6	164.9	0.8013	80.13
	120	507.4	0.0519	86.5	192.4	0.8995	89.95
	150	495.3	0.0268	91.4	149.5	0.9481	94.81

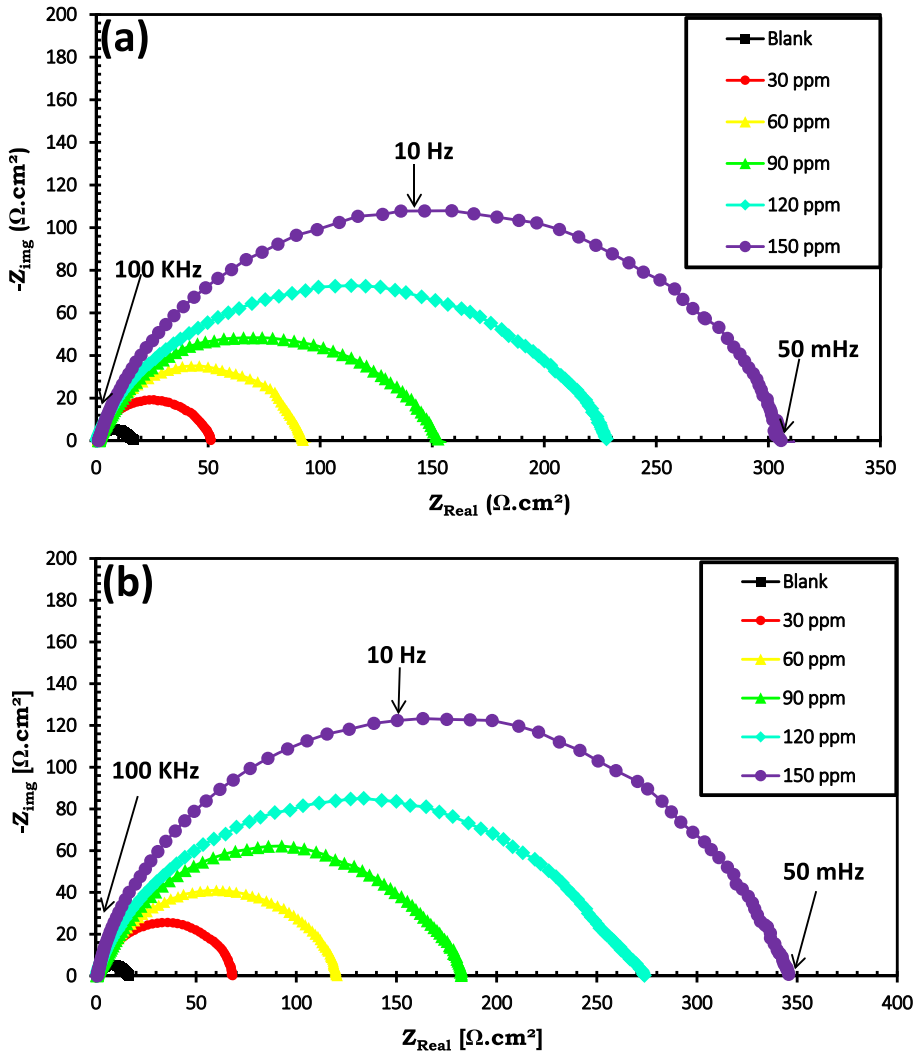

Fig. 5 Nyquist plots for CS alloy in 2 M HCl without and with various doses of compounds: **a** TAP-TPP and **b** TAP-CEQ at 25 °C

Table 3 Electrochemical parameters obtained from EIS equivalent circuit fitting of the carbon steel alloy immersed in 2 M HCl without and with various doses of inhibitors TAP-TPP and TAP-CEQ

Inhibitor	Conc. (ppm)	R_s, (Ω cm^2)	n	C_{dl}, (μF/cm^2)	R_{ct}, (Ω cm^2)	IE (%)
Blank	–	1.391	0.991	107.23	15.4	–
TAP-TPP	30	0.982	0.997	73.41	50.56	69.54
	60	1.257	0.983	40.16	92.44	83.34
	90	2.196	0.999	18.21	153.5	89.97
	120	1.409	0.984	11.67	225.6	93.17
	150	1.165	0.971	8.32	299.7	94.86
TAP-CEQ	30	1.825	0.996	48.79	67.52	77.19
	60	1.607	0.998	38.82	120.3	87.20
	90	1.263	0.992	16.45	180.8	91.48
	120	1.318	0.976	10.86	269.5	94.29
	150	1.479	0.995	6.74	346.5	95.56

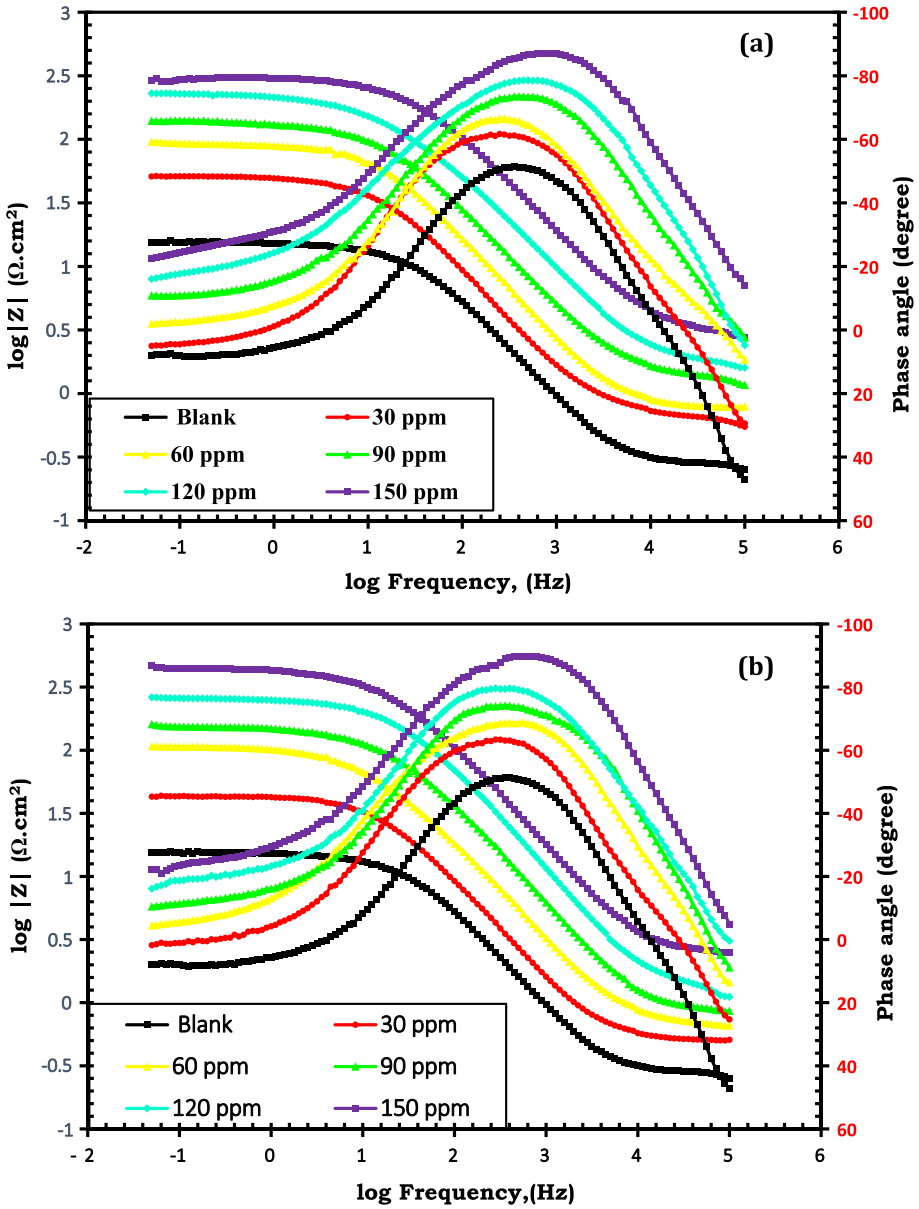

Fig. 6 Bode plots for CS alloy in 2 M HCl without and with various concentrations doses of compounds: **a** TAP-TPP and **b** TAP-CEQ at 25 °C

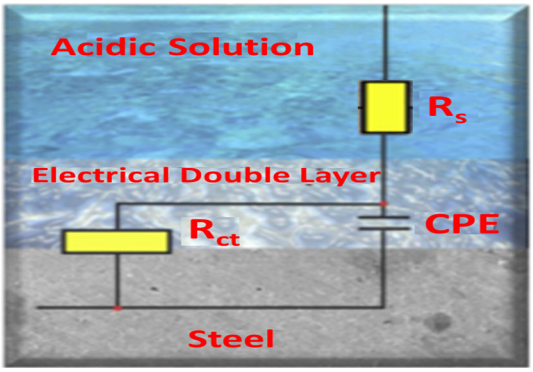

Fig. 7 Equivalent circuit used to model metal/solution interface of CS alloy in 2 M HCl without and with pyridinone derivatives

was revealed via impedance experiments. Figures 5 and 6 display the Nyquist and Bode plots of immersed CS electrodes in an acidic medium without and with several doses of these pyridinone derivatives at 25 °C. The EIS factors are recognized in Table 3. Nyquist plots in Fig. 5 showed single capacitive circles, donating that the dissolution method of CS alloy electrode in the undertaken aggressive solution without and with pyridinone derivatives undertakes by charge transfer on the surface of CS alloy/aggressive medium. Figures 5 and 6 reveals that both Nyquist and Bode plots display the unchanged style, indicating that the presence of the amino pyridinone derivatives did not change the iron dissolution mechanism while the diameter semicircles formed become greatly enhanced with increasing the concentration of pyridinone derivatives in an acidic medium [54–57]. Furthermore, the Bode plots for pyridinone derivatives in Fig. 6 indicated that the values of phase angle and the absolute impedance plots turned greater and broader with rising dose concentration of pyridinone derivatives; such changes confirm the strong ability of pyridinone particles to mitigate the dissolution of carbon steel in the acidic medium [58, 59].

To analyze the EIS outputs, a simulated equivalent circuit model was fitted to the EIS plots and is presented in Fig. 7. The values EIS parameters such as charge transfer resistance (R_{ct}), electrolyte resistance (Rs), and constant phase element (CPE) are listed in Table 3. Also, C_{dl} indicates the values of double-layer capacitance. CPE represents impedance (Z_{CPE}) and was estimated as follows [37, 60]:

$$Z_{CPE} = \frac{1}{Y_0(j\omega)^n}, \tag{4}$$

$$C_{dl} = Y_0(\omega_{max})^{n-1} \tag{5}$$

where j represents the imaginary unit, Y_0 is the value of admittance, ω represents the angular frequency, and n is the deviation index. The values of IE_{EIS} (%) from EIS parameters of the pyridinone inhibitors can be calculated by the next formula [61, 62]:

$$IE_{EIS} = \left[\frac{R_{ct} - R_{ct}^0}{R_{ct}}\right] \times 100 \tag{6}$$

where R_{ct} and R_{ct}^0 represent the values of charge transfer resistances for carbon steel without and with inhibitor doses, respectively. Results in Table 3 exposed that R_{ct} values are increased when the concentration of the pyridinone additives rises in the acidic medium. At the same time, we notice a decrease in C_{dl} values by increasing the dose of these pyridinone derivatives in an aggressive solution. This behavior was associated with the adsorption of these pyridinone derivatives on the carbon steel/solution interface, and this could lead to block corrosion interactions on CS alloy and shield the CS from other corrosive acidic attacks [63]. EIS data exposed that the values of R_{ct} rise steadily by gradually increasing the dose of these prepared compounds and this revealed a rise in the percentage inhibition effectiveness (IE %) compatible with the previously calculated PDP data. It is clear from the data obtained from various techniques used that the values of corrosion inhibition efficiency for the two compounds are increased with increasing until the optimum injection dose was reached at 150 ppm. Also, it is obvious that there is a good agreement in the order of the obtained efficiency calculated from the three techniques used in this work.

3.3.3 Adsorption Isotherm Model

For understanding the kind of adsorption interaction achieved by these synthesized pyridinone derivatives (TAP-TPP & TAP-CEQ) on CS alloy surface, various adsorption isotherms had been cheeked. In this work, Langmuir isotherm exhibited the greatest fit for these pyridinone inhibitors that is calculated by the next formula [64]:

$$\frac{C}{\theta} = \frac{1}{K_{ads}} + C \tag{7}$$

where K_{ads} represents the adsorption equilibrium constant, C is the inhibitor dose, and θ is the degree of coverage for the surface. In Fig. 8, the change of C/θ *versus* C for the undertaken compounds (TAP-TPP & TAP-CEQ provided straight lines. The obtained parameters are tabulated and listed in Table 4. The correlation coefficient (R^2) and the slope of straight lines had been found nearly 1, clarifying that the adsorption process of the pyridinone derivatives on metal surface in hydrochloric solution follows the Langmuir isotherm. The standard free energy $\left(\Delta G_{ads}^o\right)$ that was the useful parameter might be calculated by the next formula [65, 66]:

$$\Delta G_{ads}^o = -RT \ln(55.5K_{ads}) \tag{8}$$

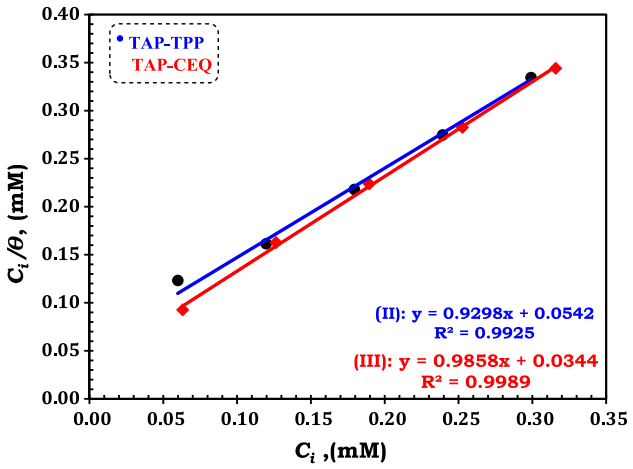

Fig. 8 Langmuir adsorption plots for the pyridinone derivatives TAP-TPP and TAP-CEQ on CS alloy in 2 M HCl

where R is the universal gas constant, T is the values of absolute temperature, and K_{ads} represents the adsorption equilibrium constant, which is estimated from the interception of the obtained straight line with the C/θ axis. The calculated values of K_{ads} and ΔG^{o}_{ads} are recorded in Table 4. Increasing the values of K_{ads} confirms the strong adsorption capacity of the pyridinone derivatives on metal surface in aggressive medium and improving mitigation of corrosion process. The obtained data in Table 4 revealed that the values of ΔG^{o}_{ads} are negative and the distribution of these derivatives on carbon steel surface takes place spontaneously. Also, data in Table 4 exposed that ΔG^{o}_{ads} values of these pyridinone derivatives ranged from − 34.29 to − 34.63 kJ Mol^{-1}, which showed that distribution of these pyridinone derivatives on CS alloy surface in the aggressive acidic medium was physicochemical adsorption (i.e., mixed physical and chemical adsorption type) [67–69].

3.4 Surface Characterization

Both SEM and EDX analyzed the images of CS alloy samples. Figure 9a–c displays the SEM images of CS alloy surfaces before and after being immersed in an acidic solution for 24 h without and with an inhibitor (TAP-CEQ) at 150 ppm. It is shown in Fig. 10a that the SEM micrograph of CS alloys displays a homogeneous, relatively smooth scratch that happened during the polishing of the CS alloy surface and at the same time without pits. Figure 10b represents the obtained SEM micrograph of the CS alloy surface in 2 M HCl solution for 24 h [70, 71]. It was found that the surface was strictly damaged and full of pits, and the surface is very rough. SEM image of carbon steel was immersed in 2 M HCl for 24 h with 150 ppm of inhibitor TAP-CEQ. Fig. 9c displays smooth, much less aggressive, and the surface morphology is enhanced. These results confirm the adsorption of this inhibitor TAP-CEQ and forming a good protective film resulting from the distribution of heteroatom (O, S, and N) on the CS surface [72].

EDX spectra of CS alloy before and after being immersed in an acidic solution for 24 h without and with 150 ppm of inhibitor TAP-CEQ represent in Fig. 9d–f. EDX spectrum of the abraded CS alloy specimen in Fig. 9d displays a very good surface morphology and a prominent Fe peak while the EDX spectrum of the CS alloy specimen in an acidic solution without inhibitor in Fig. 9e shows that the surface was highly damaged via external corrosion, oxygen signal appeared, and Fe peaks. This strongly indicates the presence of Fe_2O_3 on CS surface while the EDX spectrum of the CS alloy in 2 M HCl aggressive medium for 24 h in the presence of dose 150 ppm of compound TAP-CEQ in Fig. 9f shows a decrease in the strength of oxygen signal, and the Fe strength peak is significantly suppressed compared to peak appeared in the absence of inhibitor TAP-CEQ and the presence of N, S, and C peaks, showing the adsorption of inhibitor TAP-CEQ particles on CS surface and the creation of a good adhesive layer that prevents the surrounding aggressive medium from the attack of the metal surface [73]. These surface analyses support the data obtained from weight loss technique and electrochemical techniques.

3.5 The Assumed Corrosion Inhibition Mechanism

The pyridinone derivatives showed good corrosion inhibition properties ascribed to their affinity to be adsorbed on carbon steel alloy surface in the aggressive solution by mutual physisorption and chemisorption, as shown in Fig. 10. Pyridinone ring, thiophene group, and N atoms are strong, active binding sites in adsorption. The synthesized pyridinone derivatives can adsorb physically at the negative charge on the Cl ions and prevent corrosive ions from attacking the CS alloy surface, limiting CS alloy dissolution. Furthermore, the synthesized pyridinone derivatives can undergo

Table 4 The values of adsorption parameters obtained from adsorption isotherm of pyridinone derivatives (TAP-TPP and TAP-CEQ) for carbon steel in 2 M HCl solution

Inhibitor	Slope	Regression coefficient (R^2)	Intercept	K_{ads} (L mol^{-1})	$-\Delta G^{o}_{ads}$ (kJ mol^{-1})
TAP-TPP	0.9298	0.9925	0.0542	18,450	34.29
TAP-CEQ	0.9858	0.9989	0.0344	29,069	34.63

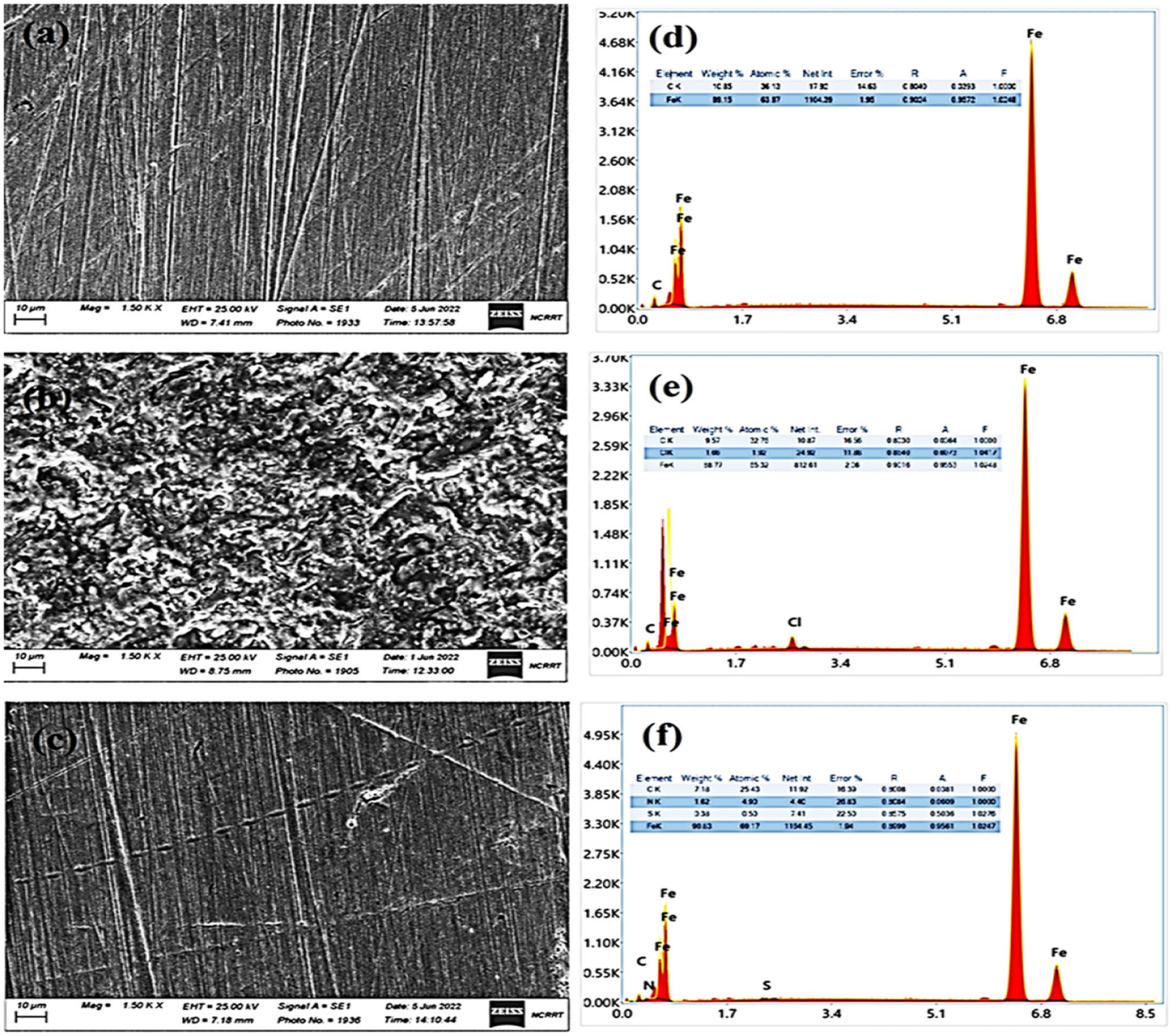

Fig. 9 SEM & EDX images for the carbon steel alloy samples in 2 M HCl; a, d = before immersion; b, e = in 2 M HCl (Blank); c, f = in 2 M HCl containing 150 ppm of inhibitor TAP-CEQ

adsorption chemically on the CS surface by their high electron density cloud. So, the structural factors found from the presence of S, O, N heteroatoms, π-electrons, cyano group (CN–), and (–C=N–) group helped to extend the double bond conjugation on the whole structure, causing better electron distribution and a more planar conformation on CS alloy [74]. So, the chemisorption is possible by forming of coordinate bonds between the lone pairs present in the pyridinone derivatives and the empty d-orbitals of Fe atoms in the carbon steel alloy surface [75, 76]. The difference between the two pyridinone particles (TAP-TPP) and (TAP-CEQ) from their chemical structure feature was responsible for their different corrosion inhibition performance, as confirmed by all techniques used in this work. Therefore, the pyridinone derivatives can lead to a strong adhesive adsorbed layer on the CS alloy surface by both physical and chemical interactions, isolating the surface of the CS alloy from an aggressive environment and then protecting it from further dissolution.

3.6 DFT Computational Study

The physical properties and calculated electron density distribution of novel prepared organic inhibitors TAP-TPP and TAP-CEQ were obtained at obtained at B3LYP/6-31G(d) level and are displayed in Fig. 11, and the values are listed in Table 5. By the specified theoretical items, the optimized geometrical structure and the frontier molecule orbitals FMOs

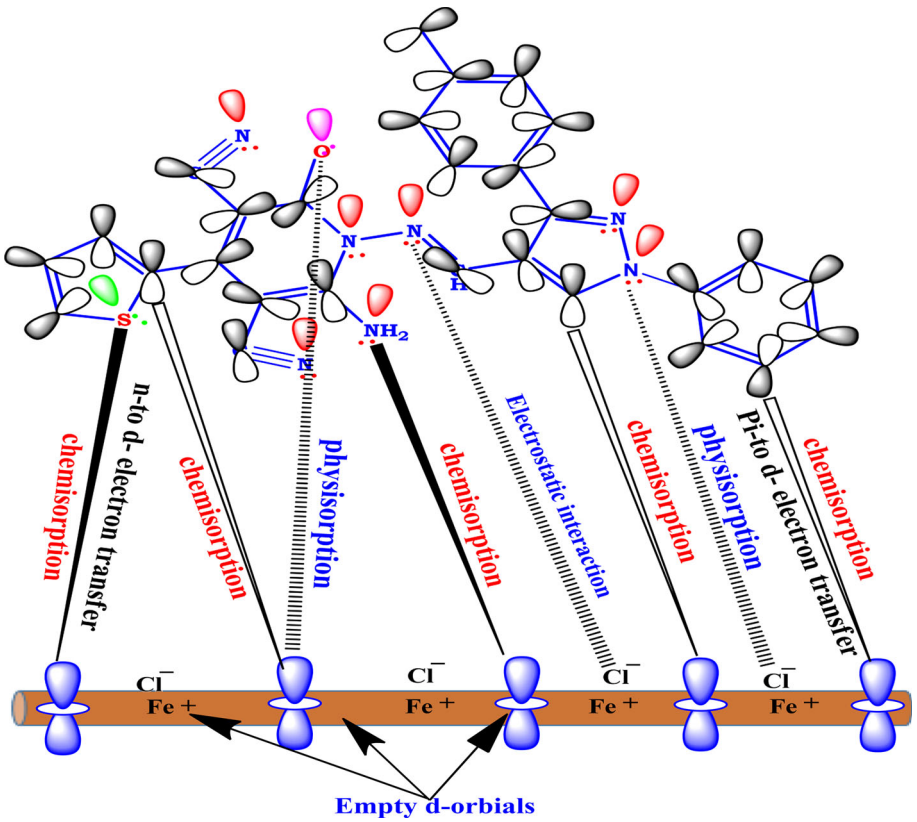

Fig. 10 Possible adsorption mechanism of inhibitor (TAP-CEQ) on carbon steel alloy surface in acidic medium

such as HOMO, LUMO, and energy band gap for the organic inhibitors were evaluated.

Firstly, every molecule possesses HOMO and LUMO levels. The HOMO level indicates the capability of molecules to release electrons, while the LUMO level reveals the capability of molecules to accept electrons. Furthermore, the organic inhibitors TAP-TPP and TAP-CEQ LUMO values were − 2.24 and − 2.53 eV, respectively. The LUMO value of TAP-CEQ inhibitors is more negative than the other inhibitors TAP-TPP. Besides, the energy gap ΔE for inhibitors TAP-TPP and TAP-CEQ was 3.89 and 3.68 eV, respectively. For clarity, the low values of energy gap for any molecule proved the easily transferred the electron from the HOMO level to the LUMO level of the same molecule. Also, this value indicates that the TAP-CEQ molecule is more applicable than TAP-TPP as an anticorrosive agent because the first is more stable and more active in accepting electrons from occupied metallic orbitals. Similarly, Table 5 represents that the TAP-CEQ inhibitor has dipole moment μ = 13.49 Debye, which is higher than those of TAP-TPP μ = 11.03 Debye and that may be due to the polar function (ethoxy CH_3CH_2O- and carbon attached to chloride atom C–Cl) in the TAP-CEQ inhibitor. This result indicates that the organic molecule with a higher dipole moment is favorable to deposit on the metal's surface area and then has greater corrosion efficiency. Moreover, the electrophilicity index ω for organic inhibitors TAP-TPP and TAP-CEQ were determined as 4.50 and 5.20 eV, respectively. This result refers to the TAP-CEQ inhibitor being accepted electron easier than TAP-TPP and more readily undergoes nucleophilic attack. Generally, all DFT computational parameters deduced that the TAP-CEQ inhibitor is more applicable than TAP-TPP as an anticorrosion inhibitor.

3.7 Comparison with Other Similar Inhibitors

In terms of structure, concentration, and inhibition efficiency values, here we compare the TAP-TPP and TAP-CEQ with other reported inhibitors. Also, Table 6 shows the values of the reported inhibitors that have similarities in their structures with TAP-TPP and TAP-CEQ, their inhibition efficiencies, and the concentrations used. The inhibition efficiency of the TAP-TPP and TAP-CEQ for carbon steel corrosion was comparative to, and even better than, many other inhibitors [26, 77–85].

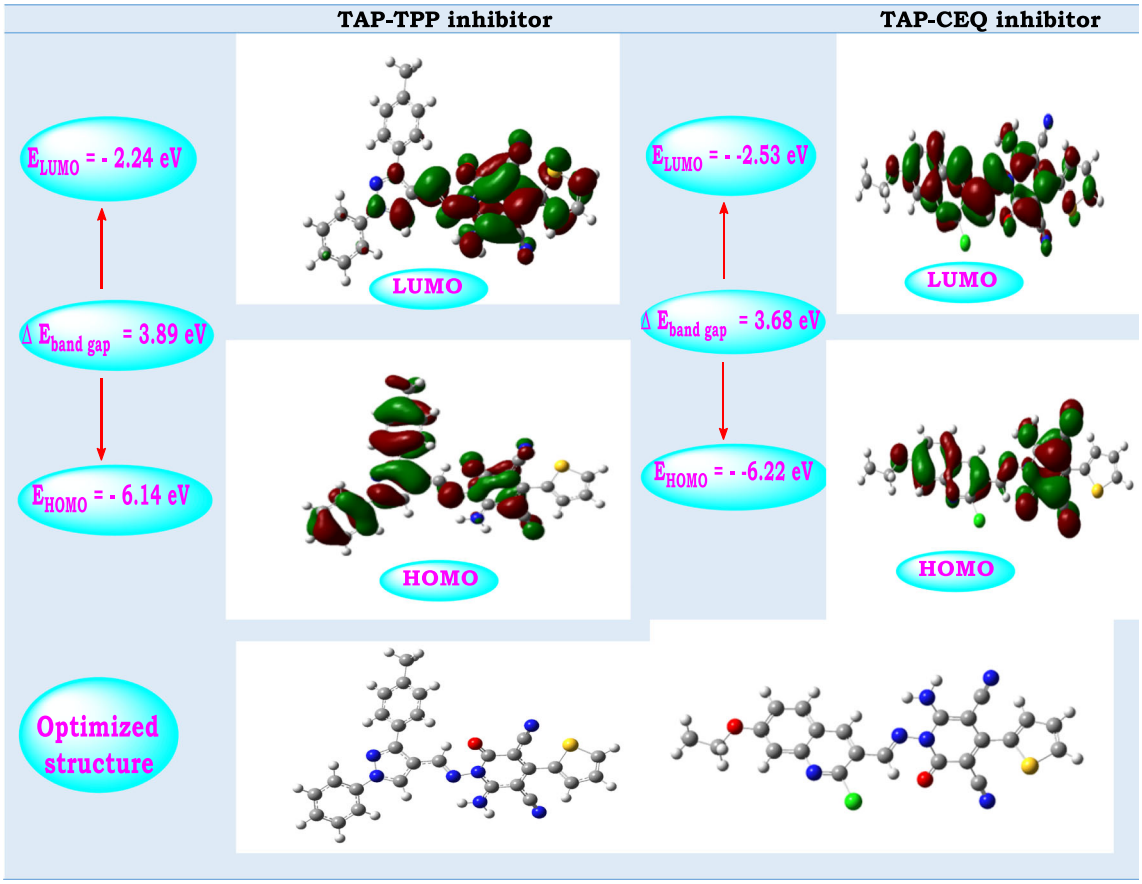

Fig. 11 Electron distributions in the HOMOs and LUMOs of the organic inhibitors TAP-TPP & TAP-CEQ and their optimized structure

Table 5 Calculated global reactivity parameters at DFT for both inhibitors (TAP-TPP and TAP-CEQ)

Inhibitor	μ (Debye)	E_{HOMO} (eV)	E_{LUMO} (eV)	ΔE (eV)	P (eV)	E_A (eV)	X (eV)	η (eV)	S (eV−1)	μ (eV)	ω (eV)
TAP-TPP	11.03	− 6.14	− 2.24	3.89	6.14	2.24	4.19	1.94	0.51	− 4.19	4.50
TAP-CEQ	13.49	− 6.22	− 2.53	3.68	6.22	2.53	4.38	1.84	0.54	− 4.38	5.20

4 Conclusion

Two novel organic inhibitors, TAP-TPP and TAP-CEQ, were synthesized, characterized, and evaluated as corrosion inhibitors in the corrosion of carbon steel in acidic medium. On the results, the following conclusions were drawn:

- The two novel organic inhibitors (TAP-TPP and TAP-CEQ) were laboratory prepared as a green chemistry synthesis using CAN as an eco-friendly catalyst with high yield (87% and 91%).
- The highest inhibition efficiency values at 150 ppm (optimum concentration) are 89.4% and 91.8% for TAP-TPP and TAP-CEQ, respectively.
- PDP data displayed that the two organic inhibitors could be classified as mixed-type inhibitors.
- EIS studies revealed the adsorption of TAP-TPP and TAP-CEQ molecules and are confirmed by increase in R_{ct} and decrease in C_{dl} values, respectively.
- The adsorption of the TAP-TPP and TAP-CEQ on MS in 2 M HCl solution follows the Langmuir isotherm, and the distribution of these organic inhibitors on the CS alloy surface in the aggressive acidic medium was physicochemical adsorption (i.e., mixed physical and chemical adsorption type) which SEM and EDX examination affirm.
- Very high negative magnitude of the ΔG_{ads} (− 34.29 to − 34.63 kJ Mol^{-1}) values showed that TAP-TPP and TAP-CEQ interact spontaneously and strongly with the metallic surface.

Table 6 Comparison of corrosion inhibition efficiency of the synthesized inhibitors (TAP-TPP and TAP-CEQ) with other reported studies

Inhibitor	Inhibition efficiency (%)	References
Sodium dodecyl benzene sulfonate	84	[26]
Three Gemini cationic surfactants	83.60, 87.30 and 90.20	[77]
Three ionic liquids based gemini cationic surfactants	90.50, 92.40 and 94	[78]
Epoxy pre-polymers as corrosion inhibitor	92.90 and 91.70	[79]
Two novel Schiff bases as inhibitors	84.00	[80]
Benzidine-based Schiff base	88.97	[81]
Novel mono azo dyes derived from 4,5,6,7-tetrahydro-1,3-benzothiazole	56.84	[82]
Novel thiophene Schiff	91.66	[83]
New azo Schiff compound	91.32	[84]
2-Pyridinecarboxaldehyde-based Schiff base	93.93	[85]
N-amino pyridinone Schiff base catalyzed with ceric(IV) ammonium nitrate	89.4 and 91.8	This study

- The results obtained from DFT computational studies such as EHOMO, ELUMO, diploe moment (μ), and electrophilicity index (ω) stated that the TAP-CEQ inhibitor is more applicable than TAP-TPP as an anticorrosion inhibitor and are in full agreement with the experimental ones.
- Finally, both novel organic inhibitors TAP-TPP and TAP-CEQ were considered excellent organic inhibitors compared to the previously reported pyridone derivatives due to the highest inhibition efficiency values at 150 ppm are 89.4% and 91.8%, respectively. The little solubility of these organic inhibitors was only the defect; it is easier in future works when papered novel ionic pyridone inhibitors.

Supplementary Information The online version contains supplementary material available at https://doi.org/10.1007/s13369-023-08073-4.

Declarations

Conflict of interest On behalf of all authors, the corresponding author states that there is no conflict of interest.

References

1. Ross, R.W.: New technology stainless steels and nickel alloys for marine applications in the year 2000 and beyond. In: Ocean. 2000 MTS/IEEE Conf. Exhib. Conf. Proc. (Cat. No.00CH37158), IEEE, n.d.: pp. 1597–1605. https://doi.org/10.1109/OCEANS.2000.882169
2. Zhao, H.; Xie, L.; Xin, C.; Li, N.; Zhao, B.; Li, L.: Effect of molybdenum content on corrosion resistance and corrosion behavior of Ti-Mo titanium alloy in hydrochloric acid. Mater. Today Commun. **34**, 105032 (2023). https://doi.org/10.1016/j.mtcomm.2022.105032
3. Kania, H.: Corrosion and anticorrosion of alloys/metals: the important global issue. Coatings **13**, 216 (2023). https://doi.org/10.3390/coatings13020216
4. Ismail, M.A.; Shaban, M.M.; Abdel-Latif, E.; Abdelhamed, F.H.; Migahed, M.A.; El-Haddad, M.N.; Abousalem, A.S.: Novel cationic aryl bithiophene/terthiophene derivatives as corrosion inhibitors by chemical, electrochemical and surface investigations. Sci. Rep. **12**, 3192 (2022). https://doi.org/10.1038/s41598-022-06863-8
5. Lgaz, H.; Chaouiki, A.; Chafiq, M.; Salghi, R.; Tachallait, H.; Bougrin, K.; Chi, H.-Y.; Kwon, C.; Chung, I.-M.: Evaluating the corrosion inhibition properties of novel 1,2,3-triazolyl nucleosides and their synergistic effect with iodide ions against mild steel corrosion in HCl: a combined experimental and computational exploration. J. Mol. Liq. **338**, 116522 (2021). https://doi.org/10.1016/j.molliq.2021.116522
6. El Arrouji, S.; Karrouchi, K.; Berisha, A.; Ismaily Alaoui, K.; Warad, I.; Rais, Z.; Radi, S.; Taleb, M.; Ansar, M.; Zarrouk, A.: New pyrazole derivatives as effective corrosion inhibitors on steel-electrolyte interface in 1 M HCl: Electrochemical, surface morphological (SEM) and computational analysis. Colloids Surf. A Physicochem. Eng. Asp. **604**, 125325 (2020). https://doi.org/10.1016/j.colsurfa.2020.125325
7. Sebhaoui, J.; El-Aoufir, Y.; El-Bakri, Y.; Bourazmi, H.; Ben-Ali, A.; Guenbour, A.; Oudda, H.; Zarrouk, A.; Essassi, E.M.: The inhibition of carbon steel corrosion in hydrochloric acid media using 2-[(5-methyl-isoxazol-3-yl)-methyl]-benzimidazole. Port. Electrochim. Acta. **39**, 213–224 (2021). https://doi.org/10.4152/pea.2021390305
8. El-Basiony, N.M.; Sliem, M.H.; Abd-Elaal, A.A.; Abdullah, A.M.; Al-Qahtani, N.H.; Zaki, E.G.; Okonkwo, P.C.; Elyan, S.S.; Shaban,

S.M.: Theoretical and experimental insights into the C-steel aqueous corrosion inhibition at elevated temperatures in 1.0 M HCl via multi-carbonyl Gemini cationic surfactants. Zeitschrift Für Phys. Chemie. (2023). https://doi.org/10.1515/zpch-2023-0219
9. Finšgar, M.; Jackson, J.: Application of corrosion inhibitors for steels in acidic media for the oil and gas industry: a review. Corros. Sci. **86**, 17–41 (2014). https://doi.org/10.1016/j.corsci.2014.04.044
10. Goyal, M.; Kumar, S.; Bahadur, I.; Verma, C.; Ebenso, E.E.: Organic corrosion inhibitors for industrial cleaning of ferrous and non-ferrous metals in acidic solutions: a review. J. Mol. Liq. **256**, 565–573 (2018). https://doi.org/10.1016/j.molliq.2018.02.045
11. Abusaif, M.S.; Fathy, M.; Abu-Saied, M.A.; Elhenawy, A.A.; Kashyout, A.B.; Selim, M.R.; Ammar, Y.A.: New carbazole-based organic dyes with different acceptors for dye-sensitized solar cells: synthesis, characterization, dssc fabrications and density functional theory studies. J. Mol. Struct. **1225**, 129297 (2021). https://doi.org/10.1016/j.molstruc.2020.129297
12. Verma, C.; Olasunkanmi, L.O.; Ebenso, E.E.; Quraishi, M.A.: Substituents effect on corrosion inhibition performance of organic compounds in aggressive ionic solutions: a review. J. Mol. Liq. **251**, 100–118 (2018). https://doi.org/10.1016/j.molliq.2017.12.055
13. Al Jahdaly, B.A.: Preparation and evaluation of new pyridone derivatives and their investigation corrosion depletion property for copper corrosion in HCl acid solution. Biomass Convers. Biorefinery. (2023). https://doi.org/10.1007/s13399-023-03765-1
14. Leçe, H.D.; Emregül, K.C.; Atakol, O.: Difference in the inhibitive effect of some Schiff base compounds containing oxygen, nitrogen and sulfur donors. Corros. Sci. **50**, 1460–1468 (2008). https://doi.org/10.1016/j.corsci.2008.01.014
15. Ismail, M.A.; Abusaif, M.S.; El-Gaby, M.S.A.; Ammar, Y.A.; Ragab, A.: A new class of anti-proliferative activity and apoptotic inducer with molecular docking studies for a novel of 1,3-dithiolo[4,5- b]quinoxaline derivatives hybrid with a sulfonamide moiety. RSC Adv. **13**, 12589–12608 (2023). https://doi.org/10.1039/D3RA01635H
16. Iroha, N.B.; Dueke-Eze, C.U.; Fasina, T.M.; Anadebe, V.C.; Guo, L.: Anticorrosion activity of two new pyridine derivatives in protecting X70 pipeline steel in oil well acidizing fluid: experimental and quantum chemical studies. J. Iran. Chem. Soc. **19**, 2331–2346 (2022). https://doi.org/10.1007/s13738-021-02450-2
17. Jeeva, M.; Susai Boobalan, M.; Prabhu, G.V.: Adsorption and anticorrosion behavior of 1-((pyridin-2-ylamino)(pyridin-4-yl)methyl)pyrrolidine-2,5-dione on mild steel surface in hydrochloric acid solution. Res. Chem. Intermed. **44**, 425–454 (2018). https://doi.org/10.1007/s11164-017-3112-3
18. More, S.V.; Sastry, M.N.V.; Yao, C.-F.: Cerium (iv) ammonium nitrate (CAN) as a catalyst in tap water: a simple, proficient and green approach for the synthesis of quinoxalines. Green Chem. **8**, 91–95 (2006). https://doi.org/10.1039/B510677J
19. Mekheimer, R.A.; Asiri, A.M.; Abdel Hameed, A.M.; Awed, R.R.; Sadek, K.U.: An efficient multicomponent, one-pot synthesis of Betti bases catalyzed by cerium (IV) ammonium nitrate (CAN) at ambient temperature. Green Process. Synth. **5**, 365–369 (2016). https://doi.org/10.1515/gps-2016-0012
20. Ramezanzadeh, M.; Sanaei, Z.; Bahlakeh, G.; Ramezanzadeh, B.: Highly effective inhibition of mild steel corrosion in 3.5% NaCl solution by green Nettle leaves extract and synergistic effect of eco-friendly cerium nitrate additive: experimental, MD simulation and QM investigations. J. Mol. Liq. **256**, 67–83 (2018). https://doi.org/10.1016/j.molliq.2018.02.021
21. Kalhor, M.; Samiei, S.; Mirshokraei, S.A.: Microwave-assisted one-step rapid synthesis of dicyano imidazoles by HNO 3 as a high efficient promoter. Green Chem. Lett. Rev. **14**, 500–508 (2021). https://doi.org/10.1080/17518253.2021.1943005
22. Zarecki, A.P.; Kolanowski, J.L.; Markiewicz, W.T.: Microwave-assisted catalytic method for a green synthesis of amides directly from amines and carboxylic acids. Molecules **25**, 1761 (2020). https://doi.org/10.3390/molecules25081761
23. Ansari, K.R.; Quraishi, M.A.; Singh, A.: Schiff's base of pyridyl substituted triazoles as new and effective corrosion inhibitors for mild steel in hydrochloric acid solution. Corros. Sci. **79**, 5–15 (2014). https://doi.org/10.1016/j.corsci.2013.10.009
24. Migahed, M.A.; Shaban, M.M.; Fadda, A.A.; Ali, T.A.; Negm, N.A.: Synthesis of some quaternary ammonium gemini surfactants and evaluation of their performance as corrosion inhibitors for carbon steel in oil well formation water containing sulfide ions. RSC Adv. **5**, 104480–104492 (2015). https://doi.org/10.1039/C5RA15112K
25. Migahed, M.A.; Nassar, I.F.: Corrosion inhibition of Tubing steel during acidization of oil and gas wells. Electrochim. Acta. **53**, 2877–2882 (2008). https://doi.org/10.1016/j.electacta.2007.10.070
26. Shaban, S.M.; Elsamad, S.A.; Tawfik, S.M.; Abdel-Rahman, A.A.-H.; Aiad, I.: Studying surface and thermodynamic behavior of a new multi-hydroxyl Gemini cationic surfactant and investigating their performance as corrosion inhibitor and biocide. J. Mol. Liq. **316**, 113881 (2020). https://doi.org/10.1016/j.molliq.2020.113881
27. El Faydy, M.; Benhiba, F.; Timoudan, N.; Lakhrissi, B.; Warad, I.; Saoiabi, S.; Guenbour, A.; Bentiss, F.; Zarrouk, A.: Experimental and theoretical examinations of two quinolin-8-ol-piperazine derivatives as organic corrosion inhibitors for C35E steel in hydrochloric acid. J. Mol. Liq. **354**, 118900 (2022). https://doi.org/10.1016/j.molliq.2022.118900
28. Beyett, T.S.; Gan, X.; Reilly, S.M.; Gomez, A.V.; Chang, L.; Tesmer, J.J.G.; Saltiel, A.R.; Showalter, H.D.: Design, synthesis, and biological activity of substituted 2-amino-5-oxo-5H-chromeno[2,3-b]pyridine-3-carboxylic acid derivatives as inhibitors of the inflammatory kinases TBK1 and IKKε for the treatment of obesity. Bioorg. Med. Chem. **26**, 5443–5461 (2018). https://doi.org/10.1016/j.bmc.2018.09.020
29. Fouda, A.E.-A.S.; El-Askalany, A.H.; Molouk, A.F.S.; Elsheikh, N.S.; Abousalem, A.S.: Experimental and computational chemical studies on the corrosion inhibitive properties of carbonitrile compounds for carbon steel in aqueous solutions. Sci. Rep. **11**, 21672 (2021). https://doi.org/10.1038/s41598-021-00701-z
30. Shaban, M.M.; Eid, A.M.; Farag, R.K.; Negm, N.A.; Fadda, A.A.; Migahed, M.A.: Novel trimeric cationic pyrdinium surfactants as bi-functional corrosion inhibitors and antiscalants for API 5L X70 carbon steel against oilfield formation water. J. Mol. Liq. **305**, 112817 (2020). https://doi.org/10.1016/j.molliq.2020.112817
31. Elgemeie, G.H.; Sayed, S.H.: Regioselective Synthesis of a New Class of N -Arylsulfonylaminated Biheterocycles. Phosphorus. Sulfur. Silicon Relat. Elem. **178**, 465–473 (2003). https://doi.org/10.1080/10426500307914
32. Migahed, M.A.; Aly, R.O.; Al-Sabagh, A.M.: Impact of gamma-ray-pre-irradiation on the efficiency of corrosion inhibition of some novel polymeric surfactants. Corros. Sci. **46**, 2503–2516 (2004). https://doi.org/10.1016/j.corsci.2004.01.013
33. Benali, O.; Zebida, M.; Benhiba, F.; Zarrouk, A.; Maschke, U.: Carbon steel corrosion inhibition in H2SO4 0.5 M medium by thiazole-based molecules: Weight loss, electrochemical, XPS and molecular modeling approaches. Colloids Surf. A Physicochem. Eng. Asp. **630**, 127556 (2021). https://doi.org/10.1016/j.colsurfa.2021.127556
34. Abusaif, M.S.; Abu-Saied, M.A.; Fathy, M.; El-Sherif, A.A.; Kashyout, A.B.; Selim, M.R.; Ammar, Y.A.: Effect of different acceptors on N-hexyl carbazole moiety for dye-sensitized solar cells: design, characterization, molecular structure, and DSSC fabrications. J. Iran. Chem. Soc. **18**, 949–960 (2021). https://doi.org/10.1007/s13738-020-02082-y

35. Yassin, A.Y.; Abdelghany, A.M.; Shaban, M.M.; Abdallah, Y.M.: Synthesis, characterization and electrochemical behavior for API 5L X70 carbon steel in 5% sulfamic acid medium using PVVH/PEMA blend filled with gold nanoparticles. Colloids Surf. A Physicochem. Eng. Asp. **635**, 128115 (2022). https://doi.org/10.1016/j.colsurfa.2021.128115
36. Shozib, I.A.; Ahmad, A.; Abdul-Rani, A.M.; Beheshti, M.; Aliyu, A.A.: A review on the corrosion resistance of electroless Ni-P based composite coatings and electrochemical corrosion testing methods. Corros. Rev. **40**, 1–37 (2022). https://doi.org/10.1515/corrrev-2020-0091
37. Hu, Z.; Meng, Y.; Ma, X.; Zhu, H.; Li, J.; Li, C.; Cao, D.: Experimental and theoretical studies of benzothiazole derivatives as corrosion inhibitors for carbon steel in 1 M HCl. Corros. Sci. **112**, 563–575 (2016). https://doi.org/10.1016/j.corsci.2016.08.012
38. Abdelsattar, M.; Badawi, A.E.-F.M.; Ibrahim, S.; Wasfy, A.F.; Tantawy, A.H.; Dardir, M.M.: Corrosion control of carbon steel in water-based mud by nanosized metallo-cationic surfactant complexes during drilling operations. ACS Omega **5**, 30881–30897 (2020). https://doi.org/10.1021/acsomega.0c03653
39. Ragab, A.; Abusaif, M.S.; Aboul-Magd, D.S.; Wassel, M.M.S.; Elhagali, G.A.M.; Ammar, Y.A.: A new exploration toward adamantane derivatives as potential anti-MDR agents: design, synthesis, antimicrobial, and radiosterilization activity as potential topoisomerase IV and DNA gyrase inhibitors. Drug Dev. Res. **83**, 1305–1330 (2022). https://doi.org/10.1002/ddr.21960
40. Ali, A.A.; Abd El-Wahab, H.; Abusaif, M.S.; Ragab, A.; Abdel-Jaid, O.A.; Eldeeb, E.A.; Ammar, Y.A.: Design, characterization, theoretical studies, and dyeing properties of new novel diazo salicylaldehyde Schiff base catalyzed with ceric(IV) ammonium nitrate (CAN) as an eco-friendly catalyst. Pigment Resin Technol. (2023). https://doi.org/10.1108/PRT-12-2022-0141
41. Ayman, R.; Abusaif, M.S.; Radwan, A.M.; Elmetwally, A.M.; Ragab, A.: Development of novel pyrazole, imidazo[1,2-b]pyrazole, and pyrazolo[1,5-a]pyrimidine derivatives as a new class of COX-2 inhibitors with immunomodulatory potential. Eur. J. Med. Chem. **249**, 115138 (2023). https://doi.org/10.1016/j.ejmech.2023.115138
42. El-Kalyoubi, S.A.; Ragab, A.; Abu Ali, O.A.; Ammar, Y.A.; Seadawy, M.G.; Ahmed, A.; Fayed, E.A.: One-pot synthesis and molecular modeling studies of new bioactive spiro-oxindoles based on uracil derivatives as SARS-CoV-2 inhibitors targeting RNA polymerase and spike glycoprotein. Pharmaceuticals. **15**, 376 (2022). https://doi.org/10.3390/ph15030376
43. Supriya, S.; Fernández-Martinez, F.: Thermal, dielectric, and surface analysis of NaDP doped glycine phosphite single crystals. J. Struct. Chem. **58**, 1668–1671 (2017). https://doi.org/10.1134/S0022476617080261
44. Supriya, S.; Kalainathan, S.; Bhagavannarayana, G.: Effect of KOH on glycine phosphite single crystal grown by the SR method. J. Phys. Chem. Solids. **74**, 70–74 (2013). https://doi.org/10.1016/j.jpcs.2012.08.001
45. Supriya, S.: Influence of sodium trimetaphosphate on glycine phosphite single crystals grown by modified thermal gradient method. J. Cryst. Growth. **577**, 126404 (2022). https://doi.org/10.1016/j.jcrysgro.2021.126404
46. Nunes, S.; Ramacciotti, F.; Neves, A.; Angelin, E.M.; Ramos, A.M.; Roldão, É.; Wallaszkovits, N.; Armijo, A.A.; Melo, M.J.: A diagnostic tool for assessing the conservation condition of cellulose nitrate and acetate in heritage collections: quantifying the degree of substitution by infrared spectroscopy. Herit. Sci. **8**, 33 (2020). https://doi.org/10.1186/s40494-020-00373-4
47. Singh, A.; Ansari, K.R.; Quraishi, M.A.; Kaya, S.: Theoretically and experimentally exploring the corrosion inhibition of N80 steel by pyrazol derivatives in simulated acidizing environment. J. Mol. Struct. **1206**, 127685 (2020). https://doi.org/10.1016/j.molstruc.2020.127685
48. Rouifi, Z.; Rbaa, M.; Abousalem, A.S.; Benhiba, F.; Laabaissi, T.; Oudda, H.; Lakhrissi, B.; Guenbour, A.; Warad, I.; Zarrouk, A.: Synthesis, characterization and corrosion inhibition potential of newly benzimidazole derivatives: combining theoretical and experimental study. Surf. Interfaces. **18**, 100442 (2020). https://doi.org/10.1016/j.surfin.2020.100442
49. El-Askalany, A.H.; Mostafa, S.I.; Shalabi, K.; Eid, A.M.; Shaaban, S.: Novel tetrazole-based symmetrical diselenides as corrosion inhibitors for N80 carbon steel in 1 M HCl solutions: experimental and theoretical studies. J. Mol. Liq. **223**, 497–508 (2016). https://doi.org/10.1016/j.molliq.2016.08.088
50. El Faydy, M.; Galai, M.; El Assyry, A.; Tazouti, A.; Touir, R.; Lakhrissi, B.; Ebn Touhami, M.; Zarrouk, A.: Experimental investigation on the corrosion inhibition of carbon steel by 5-(chloromethyl)-8-quinolinol hydrochloride in hydrochloric acid solution. J. Mol. Liq. **219**, 396–404 (2016). https://doi.org/10.1016/j.molliq.2016.03.056
51. El-Monem, M.A.; Shaban, M.M.; Migahed, M.A.; Khalil, M.M.H.: Synthesis, characterization, and computational chemical study of aliphatic tricationic surfactants as corrosion inhibitors for metallic equipment in oil fields, ACS. Omega **5**, 26626–26639 (2020). https://doi.org/10.1021/acsomega.0c03432
52. El Defrawy, A.M.; Abdallah, M.; Al-Fahemi, J.H.: Electrochemical and theoretical investigation for some pyrazolone derivatives as inhibitors for the corrosion of C-steel in 0.5 M hydrochloric acid. J. Mol. Liq. **288**, 110994 (2019). https://doi.org/10.1016/j.molliq.2019.110994
53. Saranya, J.; Sowmiya, M.; Sounthari, P.; Parameswari, K.; Chitra, S.; Senthilkumar, K.: N-heterocycles as corrosion inhibitors for mild steel in acid medium. J. Mol. Liq. **216**, 42–52 (2016). https://doi.org/10.1016/j.molliq.2015.12.096
54. Al-Sabagh, A.M.; Nasser, N.M.; El-Azabawy, O.E.; Tabey, A.E.E.: Corrosion inhibition behavior of new synthesized nonionic surfactants based on amino acid on carbon steel in acid media. J. Mol. Liq. **219**, 1078–1088 (2016). https://doi.org/10.1016/j.molliq.2016.03.048
55. Migahed, M.A.; Zaki, E.G.; Shaban, M.M.: Corrosion control in the tubing steel of oil wells during matrix acidizing operations. RSC Adv. **6**, 71384–71396 (2016). https://doi.org/10.1039/C6RA12835A
56. Deng, S.; Li, X.; Xie, X.: Hydroxymethyl urea and 1,3-bis(hydroxymethyl) urea as corrosion inhibitors for steel in HCl solution. Corros. Sci. **80**, 276–289 (2014). https://doi.org/10.1016/j.corsci.2013.11.041
57. Abdallah, Y.M.; Shalabi, K.; Bayoumy, N.M.: Eco-friendly synthesis, biological activity and evaluation of some new pyridopyrimidinone derivatives as corrosion inhibitors for API 5L X52 carbon steel in 5% sulfamic acid medium. J. Mol. Struct. **1171**, 658–671 (2018). https://doi.org/10.1016/j.molstruc.2018.06.045
58. Abd El-Lateef, H.M.; Sayed, A.R.; Shalabi, K.: Synthesis and theoretical studies of novel conjugated polyazomethines and their application as efficient inhibitors for C1018 steel pickling corrosion behavior. Surf. Interfaces. **23**, 101037 (2021). https://doi.org/10.1016/j.surfin.2021.101037
59. Daoud, D.; Douadi, T.; Issaadi, S.; Chafaa, S.: Adsorption and corrosion inhibition of new synthesized thiophene Schiff base on mild steel X52 in HCl and H2SO4 solutions. Corros. Sci. **79**, 50–58 (2014). https://doi.org/10.1016/j.corsci.2013.10.025
60. Deng, S.; Li, X.; Fu, H.: Nitrotetrazolium blue chloride as a novel corrosion inhibitor of steel in sulfuric acid solution. Corros. Sci. **52**, 3840–3846 (2010). https://doi.org/10.1016/j.corsci.2010.07.020
61. Ichchou, I.; Larabi, L.; Rouabhi, H.; Harek, Y.; Fellah, A.: Electrochemical evaluation and DFT calculations of aromatic sulfonohydrazides as corrosion inhibitors for XC38 carbon steel in

acidic media. J. Mol. Struct. **1198**, 126898 (2019). https://doi.org/10.1016/j.molstruc.2019.126898
62. Zhang, M.; Liu, Y.; Li, D.; Cui, X.; Wang, L.; Li, L.; Wang, K.: Electrochemical impedance spectroscopy: a new chapter in the fast and accurate estimation of the state of health for lithium-ion batteries. Energies **16**, 1599 (2023). https://doi.org/10.3390/en16041599
63. Shaban, S.M.; Elbhrawy, M.F.; Fouda, A.S.; Rashwan, S.M.; Ibrahim, H.E.; Elsharif, A.M.: Corrosion inhibition and surface examination of carbon steel 1018 via N-(2-(2-hydroxyethoxy)ethyl)-N, N-dimethyloctan-1-aminium bromide in 1.0 M HCl. J. Mol. Struct. **1227**, 129713 (2021). https://doi.org/10.1016/j.molstruc.2020.129713
64. Hefnawy, M.A.; Fadlallah, S.A.; El-Sherif, R.M.; Medany, S.S.: Synergistic effect of Cu-doped NiO for enhancing urea electrooxidation: comparative electrochemical and DFT studies. J. Alloys Compd. **896**, 162857 (2022). https://doi.org/10.1016/j.jallcom.2021.162857
65. Li, X.; Deng, S.; Fu, H.: Triazolyl blue tetrazolium bromide as a novel corrosion inhibitor for steel in HCl and H_2SO_4 solutions. Corros. Sci. **53**, 302–309 (2011). https://doi.org/10.1016/j.corsci.2010.09.036
66. Farag, A.A.; Ali, T.A.: The enhancing of 2-pyrazinecarboxamide inhibition effect on the acid corrosion of carbon steel in presence of iodide ions. J. Ind. Eng. Chem. **21**, 627–634 (2015). https://doi.org/10.1016/j.jiec.2014.03.030
67. Tourabi, M.; Nohair, K.; Traisnel, M.; Jama, C.; Bentiss, F.: Electrochemical and XPS studies of the corrosion inhibition of carbon steel in hydrochloric acid pickling solutions by 3,5-bis(2-thienylmethyl)-4-amino-1,2,4-triazole. Corros. Sci. **75**, 123–133 (2013). https://doi.org/10.1016/J.CORSCI.2013.05.023
68. Solmaz, R.: Investigation of adsorption and corrosion inhibition of mild steel in hydrochloric acid solution by 5-(4-Dimethylaminobenzylidene)rhodanine. Corros. Sci. **79**, 169–176 (2014). https://doi.org/10.1016/j.corsci.2013.11.001
69. Abdallah, M.; Al-Tass, H.M.; Jahdaly, B.A.A.L.; Fouda, A.S.: Inhibition properties and adsorption behavior of 5-arylazothiazole derivatives on 1018 carbon steel in 0.5 M H2SO4 solution. J. Mol. Liq. **216**, 590–597 (2016)
70. Stübner, K.; Jonckheere, R.; Ratschbacher, L.: The densities and dimensions of recoil-track etch pits in mica. Chem. Geol. **404**, 52–61 (2015). https://doi.org/10.1016/j.chemgeo.2015.03.023
71. Supriya, S.; Dos Santos-García, A.J.; Fernández-Martinez, F.: Growth of NaDP-GPI single crystal and its analysis on basis of HRXRD, optical and mechanical studies. Mater. Lett. **128**, 114–116 (2014). https://doi.org/10.1016/j.matlet.2014.04.139
72. Negm, N.A.; Migahed, M.A.; Farag, R.K.; Fadda, A.A.; Awad, M.K.; Shaban, M.M.: High performance corrosion inhibition of novel tricationic surfactants on carbon steel in formation water: electrochemical and computational evaluations. J. Mol. Liq. **262**, 363–375 (2018). https://doi.org/10.1016/j.molliq.2018.04.092
73. Farag, A.A.: Oil-in-water emulsion of a heterocyclic adduct as a novel inhibitor of API X52 steel corrosion in acidic solution. Corros. Rev. **36**, 575–588 (2018). https://doi.org/10.1515/corrrev-2018-0002
74. Murmu, M.; Saha, S.K.; Murmu, N.C.; Banerjee, P.: Effect of stereochemical conformation into the corrosion inhibitive behaviour of double azomethine based Schiff bases on mild steel surface in 1 mol L−1 HCl medium: an experimental, density functional theory and molecular dynamics simulation study. Corros. Sci. **146**, 134–151 (2019). https://doi.org/10.1016/j.corsci.2018.10.002
75. Hsissou, R.; Benhiba, F.; Dagdag, O.; El Bouchti, M.; Nouneh, K.; Assouag, M.; Briche, S.; Zarrouk, A.; Elharfi, A.: Development and potential performance of prepolymer in corrosion inhibition for carbon steel in 1.0 M HCl: outlooks from experimental and computational investigations. J. Colloid Interface Sci. **574**, 43–60 (2020). https://doi.org/10.1016/j.jcis.2020.04.022
76. Zhang, Q.B.; Hua, Y.X.: Corrosion inhibition of mild steel by alkylimidazolium ionic liquids in hydrochloric acid. Electrochim. Acta. **54**, 1881–1887 (2009). https://doi.org/10.1016/j.electacta.2008.10.025
77. Kellou-Kerkouche, F.; Benchettara, A.; Amara, S.-E.: Anionic surfactant as a corrosion inhibitor for synthesized ferrous alloy in acidic solution. J. Mater. **2013**, 1–11 (2013). https://doi.org/10.1155/2013/903712
78. Tawfik, S.M.: Ionic liquids based gemini cationic surfactants as corrosion inhibitors for carbon steel in hydrochloric acid solution. J. Mol. Liq. **216**, 624–635 (2016). https://doi.org/10.1016/j.molliq.2016.01.066
79. Dagdag, O.; Safi, Z.; Hsissou, R.; Erramli, H.; El Bouchti, M.; Wazzan, N.; Guo, L.; Verma, C.; Ebenso, E.E.; El Harfi, A.: Epoxy pre-polymers as new and effective materials for corrosion inhibition of carbon steel in acidic medium: computational and experimental studies. Sci. Rep. **9**, 11715 (2019). https://doi.org/10.1038/s41598-019-48284-0
80. Padash, R.; Rahimi-Nasrabadi, M.; Shokuhi Rad, A.; Sobhani-Nasab, A.; Jesionowski, T.; Ehrlich, H.: A theoretical study of two novel Schiff bases as inhibitors of carbon steel corrosion in acidic medium. Appl. Phys. A. **125**, 78 (2019). https://doi.org/10.1007/s00339-018-2376-9
81. Bedair, M.A.; Soliman, S.A.; Bakr, M.F.; Gad, E.S.; Lgaz, H.; Chung, I.-M.; Salama, M.; Alqahtany, F.Z.: Benzidine-based Schiff base compounds for employing as corrosion inhibitors for carbon steel in 1.0 M HCl aqueous media by chemical, electrochemical and computational methods. J. Mol. Liq. **317**, 114015 (2020). https://doi.org/10.1016/j.molliq.2020.114015
82. Mallikarjuna, N.M.; Keshavayya, J.; Prasanna, B.M.; Praveen, B.M.; Tandon, H.C.: Synthesis, characterization, and anti-corrosion behavior of novel mono azo dyes derived from 4,5,6,7-tetrahydro-1,3-benzothiazole for mild steel in acid solution. J. Bio- Tribo-Corros. **6**, 9 (2020). https://doi.org/10.1007/s40735-019-0306-9
83. Tezcan, F.; Yerlikaya, G.; Mahmood, A.; Kardaş, G.: A novel thiophene Schiff base as an efficient corrosion inhibitor for mild steel in 1.0 M HCl: electrochemical and quantum chemical studies. J. Mol. Liq. **269**, 398–406 (2018). https://doi.org/10.1016/j.molliq.2018.08.025
84. Abdulridha, A.A.; Albo Hay Allah, M.A.; Makki, S.Q.; Sert, Y.; Salman, H.E.; Balakit, A.A.: Corrosion inhibition of carbon steel in 1 M H2SO4 using new Azo Schiff compound: electrochemical, gravimetric, adsorption, surface and DFT studies. J. Mol. Liq. **315**, 113690 (2020). https://doi.org/10.1016/j.molliq.2020.113690
85. Li, X.-L.; Xie, B.; Feng, J.-S.; Lai, C.; Bai, X.-X.; Li, T.; Zhang, D.-L.; Mou, W.-Y.; Wen, L.; Gu, Y.-T.: 2-Pyridinecarboxaldehyde-based Schiff base as an effective corrosion inhibitor for mild steel in HCl medium: experimental and computational studies. J. Mol. Liq. **345**, 117032 (2022). https://doi.org/10.1016/j.molliq.2021.117032